

Statistics of Cosmological Black Hole Jet Sources: Blazar Predictions for GLAST

Charles D. Dermer¹

ABSTRACT

A study of the statistics of cosmological black-hole jet sources is applied to EGRET blazar data, and predictions are made for GLAST. Black-hole jet sources are modeled as collimated relativistic outflows with radiation beamed along the jet axis due to strong Doppler boosting. The comoving density dependence of the blazar formation rate (BFR) is assumed to follow the cosmic star formation history or cosmic evolution of IR-luminous galaxies. A parameter study of blazar redshift and size distributions is presented using synchrotron and external Compton (EC) beaming factors for different BFRs. The redshift and luminosity distributions of gamma-ray blazars observed with EGRET, separated into BL Lac object (BL) and flat spectrum radio quasar (FSRQ) distributions, are fit with monoparametric functions for the distributions of the jet Lorentz factor Γ , comoving directional power ℓ'_e , and spectral slope. The detection characteristics of a telescope are approximated by its νF_ν sensitivity threshold f_ϵ at photon frequency $\nu = m_e c^2 \epsilon / h$. Values of Γ and ℓ'_e that fit the data for FSRQs and BLs are estimated. Based on the EGRET observations, predictions for the detectability of blazars with GLAST are made. GLAST would detect a much larger fraction of BLs in its sample than found with EGRET but that BL evolution must be negative in order that BLs not overproduce the γ -ray background. The FSRQ contribution to the EGRET extragalactic γ -ray background is estimated at the level of $\approx 30\%$. EGRET and GLAST sensitivities to blazar flares are considered in the optimal case, and a GLAST analysis method for blazar flares is outlined.

Subject headings: AGNs: blazars—black holes—gamma-ray bursts

1. Introduction

Population studies of black-hole jet sources, which include blazars, gamma-ray bursts and microquasars, are difficult because of the unknown emission processes and beaming patterns of the relativistic jets. Moreover, the density and luminosity evolution of black-hole jet sources through cosmic time is uncertain. Here we develop a method to treat the statistics of black-hole jet sources using on the γ -ray data alone. Although the focus of this study is radio galaxies and blazars, the method can also be applied to GRBs.

The interest in population statistics of blazar sources is that an accurate determination of source density evolution is needed to identify parent populations (Urry & Padovani 1995), to chart black-hole formation and growth throughout the history of the universe (Böttcher & Dermer 2002; Cavaliere & D'Elia 2002; Maraschi & Tavecchio 2003), and to assess the contribution of black-hole jet sources to the diffuse isotropic γ -ray background (DIGRB) (Sreekumar et al. 1998; Strong et al. 2004). The DIGRB consists of the diffuse extragalactic γ -ray background (DEGRB) and an uncertain contribution from quasi-isotropic Galactic γ rays

¹E. O. Hulbert Center for Space Research, Code 7653 Naval Research Laboratory, Washington, D.C. 20375-5352; dermer@gamma.nrl.navy.mil

produced, for example, by Compton-scattered radiations from cosmic-ray electrons. The DIGRB impedes blazar flare discovery by providing an unavoidable background.

Soon after the recognition of the γ -ray blazar class with EGRET (Fichtel et al. 1994), γ -ray blazar population studies were undertaken. Chiang et al. (1995) noted that analysis of $\langle V/V_{max} \rangle$ values for EGRET blazars required cosmic evolution of source properties. Chiang & Mukherjee (1998) assumed a radio/ γ -ray correlation for luminosity evolution and parameterized density evolution. They obtained best-fit values through the maximum likelihood method that implied that the AGN contribution to the DEGRB was at the level of $\approx 25\%$.

Stecker & Salamon (1996) also postulated a radio/ γ -ray connection, and tried to correct for the duty cycle and γ -ray spectral hardening of flaring states. They found that essentially 100% of the EGRET DEGRB (Sreekumar et al. 1998) arises from unresolved blazars and AGN. They did not, however, fit the blazar redshift distribution, which would have provided a check for the model. The crucial underlying assumption of these approaches, which have been developed in further detail in recent work by Giommi et al. (2006) and Narumoto & Totani (2006), is that there is a close connection between the radio and γ -ray properties of blazars. This is apparently true of the flat spectrum radio quasars (FSRQs), which are well represented by the flat spectrum radio sources in the 5 GHz, > 1 Jy Kühr et al. (1981) catalog, and also for radio-selected BL Lac objects (BLs), but less so for the X-ray selected BLs. It is therefore necessary to distinguish between the very different properties and histories of FSRQs and BLs and their separate contributions to the DEGRB (for a calculation of the DEGRB from FR1 radio galaxies, which are thought to be the parent population of BLs, see Stawarz et al. 2006).

The approach followed here is to avoid the uncertainties in the radio/ γ -ray connection, and to consider a physical model for blazars, subdivided into (at least) the BL and FSRQ classes. Predictions arising from the physical model stem from a parameter set that gives acceptable agreement with EGRET γ -ray observations of blazar redshift and flux size distributions. Such predictions depend on the beaming factor, radiation process, and blazar formation rate (BFR) history. If this cannot be accomplished with a mono-parameter model for blazars, then parameter distributions or luminosity evolution must be considered. The connection of the γ -ray blazar properties to properties at radio, X-ray, and other wavelength can be obtained as a final (model-dependent) check on the model.

Employing such a method, Mücke & Pohl (2000) developed a physical blazar model to fit the EGRET blazar data. They concluded that $\approx 70 - 90\%$ of the DEGRB produced by unresolved AGNs is made by FR1s and BLs. In a related study, Dermer & Davis (2000) noted that the smaller average redshift of BLs than FSRQs means that the more sensitive surveys planned with the *Gamma ray Large Area Space Telescope* (GLAST)¹, would detect a larger fraction of BLs compared to FSRQs than was detected with EGRET.

Here we develop this approach in more detail, using a simple blazar model based on our understanding of the underlying radiation physics and relativistic beaming of blazars. Our model is simpler than that of Mücke & Pohl (2000) by not treating radiative cooling, but has the advantage of providing simple expressions for the statistics of cosmological jet sources. The results are fit to the redshift and peak luminosity distributions of EGRET gamma-ray blazars, and used to make predictions for GLAST.

Radio galaxies and blazars are the focus of this work. With caveats, the formalism can also be applied to GRBs and microquasars. A particular difference is that our analysis assumes a jet opening angle $\theta_j \lesssim 1/\Gamma$,

¹glast.gsfc.nasa.gov, www-glast.stanford.edu

where Γ is the bulk Lorentz factor of the outflow. This source model represents a quasi-spherical (in the comoving frame) plasma blob, or a blast wave with $\theta_j \lesssim 1/\Gamma$, but is quite unlike a highly relativistic blast-wave shell with $\theta_j \gg 1/\Gamma$ used to model the prompt phase of GRBs.

Section 2 gives the selection criteria for the EGRET blazar data used. The equations for the analysis are presented in Section 3, and results of the parameter study are described in Section 4. Predictions for GLAST are presented in Section 5, and we summarize in Section 6. Sensitivities of EGRET and GLAST to blazar flares, expressions for optimal sensitivities, and a discussion of a GLAST analysis strategy for blazar populations are given in the Appendix.

2. Sample

Crucial to making a proper comparison of a model to EGRET blazar data is to choose a sample that is unbiased with respect to exposure and background. For example, exposure to the region around 3C 273 and 3C 279 was much longer than average over the lifetime of EGRET, so blazars found in these pointings would be detected to much smaller flux thresholds than on average. Likewise, blazars in the vicinity of the galactic plane would have to be much brighter than high-latitude sources to be detected above the diffuse galactic γ -ray emission.

The 18 month all-sky EGRET survey (Fichtel et al. 1994), which ran from 1991 May to 1992 November, had roughly uniform exposure over all parts of the sky. Thirty-eight AGN identifications were reported in this catalog. Additional analysis of the Phase 1 data, as reported in the 3EG catalog (Hartman et al. 1999), revealed numerous additional detections of AGNs during Phase 1.

We have identified all the high-confidence blazars listed in the Third EGRET catalog that also appear during the 18 month all-sky survey, during which all parts of the sky receive roughly uniform exposure. The sample we use consists of 60 high-confidence gamma-ray blazars, consisting of 14 BLs and 46 FSRQs. We exclude sources within 10° of the Galactic plane, and use source catalogs (Padovani & Giommi 1995; Perlman 1996) to establish BL identifications. The peak 100 MeV – 5 GeV νF_ν fluxes, denoted $f_\epsilon(100 \text{ MeV} - 5 \text{ GeV})$, were used to construct the FSRQ and BL size distributions.

Table 1 lists the sources from the Third EGRET catalog (Hartman et al. 1999) used in this study and their classifications. The γ -ray blazar sample, binned by redshift and grouped into BLs and FSRQs, is plotted in Fig. 1. Fig. 2 shows the FSRQ and BL size distributions. EGRET had sensitivity for 10^6 s (two-week) pointings to high-latitude blazars at a νF_ν flux threshold $f_\epsilon(100 \text{ MeV} - 5 \text{ GeV}) \cong 10^{-10} \text{ ergs cm}^{-2} \text{ s}^{-1}$, or a number threshold of $\approx 15 \times 10^{-8} \text{ ph}(E > 100 \text{ MeV}) \text{ cm}^{-2} \text{ s}^{-1}$.

The BLs and FSRQs display very different γ -ray properties. The BLs are less numerous and closer, with an average redshift $z \sim 0.5$, whereas the FSRQ distribution peaks at $z \sim 1$, and shows a tail reaching to $z \sim 2.3$. There are $\approx 5 \times$ as many FSRQs as BLs per unit peak flux in the EGRET range ($\gtrsim 10^{-10} \text{ ergs cm}^{-2} \text{ s}^{-1}$). The FSRQ flares are $\sim 1 - 2$ orders of magnitude more luminous than the BL flares (inset to Fig. 2). The FSRQ blazar flares have powers as large as $\approx 10^{50} \text{ ergs s}^{-1}$, with BL flares as powerful as $\approx 10^{49} \text{ ergs s}^{-1}$.

More detailed studies of the redshift and size distribution can be made with the EGRET data (R. Romani, private communication, 2006) based on surveys to identify γ -ray blazars (Sowards-Emmerd et al. 2005). These studies also show that the mean redshift of FSRQs is ≈ 1 , and that both the BL and FSRQ populations have tails to high redshifts. The highest redshift γ -ray blazar candidate has $z = 5.47$ (Romani

et al. 2004). The treatment here is illustrative, and the approach can be refined with larger data bases from EGRET and, of course, GLAST. The great asset of GLAST, besides its good sensitivity and large field-of-view (FOV) is that, in the scanning mode, it provides essentially uniform exposure over the whole sky.

A more precise discussion of threshold fluxes needs to be made at this point. A γ -ray telescope measures, with $\sim 10\%$ uncertainty, the energy E of an incoming γ ray. For tens of counts or less, there are not enough photons to construct a flare spectrum, and one measures an average photon energy $\langle E \rangle$ (contaminated with background photons) and a νF_ν flux $f_\epsilon(E_1, E_2)$ between photon energies E_1 and E_2 . Typically, $E_1 = 100$ MeV and $E_2 = 5$ GeV for EGRET. For optimal significance in detection of blazars with GLAST or EGRET, an energy ranges that depend on the source spectral hardness should be used (Appendix A).

For comparison, a theoretical model calculates a νF_ν spectral flux f_ϵ at photon energy ϵ that does not take into account bolometric corrections. To compare a theoretical model with data, the model value $f_\epsilon \approx f_\epsilon(E_1, E_2)/b_c$, where b_c is a bolometric correction that is larger for spectra that are flatter in a νF_ν representation. In our model comparison with EGRET data, we take $f_\epsilon \cong 2 \times 10^{-11}$ ergs cm^{-2} s^{-1} , corresponding to a threshold EGRET flux $f_\epsilon(100 \text{ MeV}, 5 \text{ GeV}) \cong 10^{-10}$ ergs cm^{-2} s^{-1} , that is, $b_c \approx 1/5$.

3. Analysis

We employ a simplified version of the standard model for blazars described by Dermer & Gehrels (1995) (see also, e.g., Sikora et al. 1997). A relativistically moving plasmoid ejected from a black-hole engine has accelerated within it, either through internal or external shocks or otherwise, a power-law distribution of quasi-isotropic ultra-relativistic electrons with number index p . In its proper frame, a plasmoid is assumed to entrain a randomly oriented magnetic field with mean strength B . The nonthermal electrons emit synchrotron or Thomson radiation that is Doppler boosted by the effects of the relativistic motion. For the calculations shown here, we use the synchrotron beaming factor $\propto \delta_D^{(5+p)/2}$, where the Doppler factor $\delta_D = [\Gamma(1 - \beta \cos \theta)]^{-1}$, and the external Compton (EC) beaming factor $\propto \delta_D^{3+p}$ (Dermer 1995), which also holds for scattering in the Klein-Nishina regime (Georganopoulos et al. 2001). Here Γ is the bulk Lorentz factor of the plasma blob, $\beta = \sqrt{1 - \Gamma^{-2}}$, $\alpha = (p-1)/2 = \alpha_{ph} - 1$ is the energy spectral index of the radiation (α_{ph} is the number index), and θ is the angle between the jet and line-of-sight directions. Continuous outflow scenarios produce a beaming pattern weaker by one power (Lind & Blandford 1985)).

3.1. Cosmology of Nonthermal Sources

Consider a power-law distribution of electrons with low- and high-energy cutoffs, so that the total number distribution of nonthermal electrons within the plasmoid is described by

$$N'_e(\gamma) = K_e \gamma^{-p} H(\gamma; \gamma_1, \gamma_2). \quad (1)$$

Note that p is the number index of the emitting electrons, and could be different from the injection index if cooling is important. Normalizing to the total comoving electron energy $W'_e = m_e c^2 \int_1^\infty d\gamma \gamma N'_e(\gamma)$ implies

$$K_e = \frac{(p-2)W'_e}{m_e c^2} (\gamma_1^{2-p} - \gamma_2^{2-p})^{-1} \rightarrow \frac{(p-2)W'_e \gamma_1^{p-2}}{m_e c^2}, \text{ when } p > 2, \gamma_2 \gg \gamma_1. \quad (2)$$

Cooling will introduce a break in the electron spectrum (Mücke & Pohl 2000), but most blazars, including bright blazars, are well fit by a single power law, suggesting that the single power-law approximation is

adequate for a treatment of blazar statistics.

The νF_ν nonthermal synchrotron radiation spectrum for a comoving isotropic power-law distribution of electrons entrained in a randomly oriented magnetic field is given in the δ -function approximation by the expression

$$f_\epsilon^s \cong \frac{\delta_D^4}{6\pi d_L^2} c\sigma_T U_B \gamma_s^3 N'_e(\gamma_s), \quad \gamma_s = \sqrt{\frac{\epsilon_z}{\delta_D b}}, \quad (3)$$

where the luminosity distance for a flat Λ CDM universe is

$$d_L(z) = \frac{c}{H_0} (1+z) \int_0^z dz' \frac{1}{\sqrt{\Omega_m(1+z')^3 + \Omega_\Lambda}}, \quad (4)$$

$U_B = B^2/8\pi$ is the magnetic-field energy density in the jet plasma, $b \equiv B/B_{cr}$, and $B_{cr} = m_e^2 c^3/e\hbar$ is the critical magnetic field.

The νF_ν spectrum of jet electrons that Thomson scatter an external quasi-isotropic monochromatic radiation field with stationary (explosion)-frame dimensionless photon energy $\epsilon_* = 10^{-4}\epsilon_{-4}$ and stationary frame energy density U_* is

$$f_\epsilon^{EC} \cong \frac{\delta_D^6}{6\pi d_L^2} c\sigma_* U_* \gamma_C^3 N'_e(\gamma_C), \quad \gamma_C = \frac{1}{\delta_D} \sqrt{\frac{\epsilon_z}{2\epsilon_*}} \quad (5)$$

(Dermer 1995); (see Dermer & Schlickeiser 2002, for expressions for the Thomson-scattered accretion-disk radiation fields). Restriction to the Thomson regime implies that $\epsilon_z \lesssim 1/(8\epsilon_*)$, so that a target 5 eV UV radiation field would display effects from the onset of the KN decline in the cross section at $E \gtrsim 6$ GeV/(1 + z). A more accurate treatment for GLAST analysis will have to consider the effects of the KN decline on the statistics.

The νF_ν synchrotron self-Compton (SSC) radiation spectrum in the δ -function approximation is

$$f_\epsilon^{SSC} \cong \frac{\delta_D^4}{9\pi d_L^2} \frac{c\sigma_T r_b U_B K_e^2}{V'_b} \gamma_s^{3-p} \Sigma_C, \quad (6)$$

where the Compton-synchrotron logarithm $\Sigma_c = \ln(a_{max}/a_{min})$, $a_{max} = \min(b\gamma_2^2, \epsilon'/\gamma_1^2, \epsilon'^{-1})$, $a_{min} = \max(b\gamma_1^2, \epsilon'/\gamma_2^2)$, and $\epsilon' = \epsilon_z/\delta_D$ (Gould 1979; Dermer et al. 1997). The SSC process has a similar dependence as the synchrotron process—though a curvature in the spectrum is produced by Σ_c —but with a different coefficient that depends on the physical size of the radiating plasma.

We write eqs. (3) – (6) as

$$f_\epsilon^{proc} = \frac{\ell'_e}{d_L^2} \delta_D^q \epsilon_z^{\alpha_\nu}, \quad (7)$$

where $\alpha_\nu = (3-p)/2$ is the νF_ν spectral index, the directional comoving luminosity

$$\ell'_e(\text{ergs s}^{-1}\text{sr}^{-1}) = \frac{K_e c \sigma_T}{6\pi} \begin{cases} U_{B_{cr}} b^{(p+1)/2}, & \text{synchrotron} \\ \frac{K_e \sigma_T}{2\pi r_b'^2} U_{B_{cr}} \Sigma_C b^{(p+1)/2}, & \text{SSC} \\ U_* (2\epsilon_*)^{(p-3)/2}, & \text{EC} \end{cases}$$

the beaming factor index

$$q = \begin{cases} (p+5)/2, & \text{synchrotron, SSC} \\ p+3, & \text{EC} \end{cases},$$

and $U_{B_{cr}} \equiv B_{cr}^2/8\pi$.

The event rate per sr for bursting sources in a Λ CDM cosmology (or the directional event rate) is

$$\frac{d\dot{N}}{d\Omega} = \frac{c}{H_0} \frac{d_L^2 \dot{n}_{com}(L', \alpha; z) dL' d\alpha dz}{(1+z)^3 \sqrt{\Omega_m(1+z)^3 + \Omega_\Lambda}}, \quad (8)$$

where $\dot{n}_{com}(L', \alpha; z)$ is the differential rate density of sources with comoving luminosity L' and spectral parameter α at redshift z . From the WMAP data (Spergel et al. 2003), we take $\Omega_m = 0.27$, $\Omega_\Lambda = 0.73$, and Hubble's constant $H_0 = 72 \text{ km s}^{-1} \text{ Mpc}^{-1}$. The directional event rate (i.e., number count) of steady sources is

$$\frac{dN}{d\Omega} = \frac{c}{H_0} \frac{d_L^2 n_{com}(L', \alpha; z) dL' d\alpha dz}{(1+z)^2 \sqrt{\Omega_m(1+z)^3 + \Omega_\Lambda}}, \quad (9)$$

and $n_{com}(L', \alpha; z)$ is the differential source density.

In an integral formulation for bursting sources (Dermer 1992), the observed directional event rate above the νF_ν spectral flux threshold \hat{f}_ϵ of the telescope is

$$\begin{aligned} \frac{d\dot{N}(>\hat{f}_\epsilon)}{d\Omega} &= \frac{c}{H_0} \int_{\hat{f}_\epsilon}^{\infty} df_\epsilon \int_0^{\infty} dW'_e \int_{-\infty}^{\infty} dp \int_1^{\infty} d\Gamma \int_0^1 d\mu \\ &\times \int_0^{\infty} dz \frac{d_L^2(z) \dot{n}_{com}(W'_e, p, \Gamma; z)}{(1+z)^3 \sqrt{\Omega_m(1+z)^3 + \Omega_\Lambda}} \delta[f_\epsilon - f_\epsilon^{proc}(W'_e, p, \Gamma, \mu, f_\epsilon)]. \end{aligned} \quad (10)$$

Here f_ϵ^{proc} is the νF_ν flux for the process under consideration, with synchrotron, EC, and SSC fluxes written as eq. (7). Here $\mu = \cos\theta$, and W'_e is defined after eq. (1). For a better treatment of detector response, one should calculate a photon-energy integration over effective area, rather than describing a γ -ray telescope by a νF_ν flux sensitivity \hat{f}_ϵ at a single photon energy $\bar{\epsilon}$. (This calls for effective area calculations for GLAST in a standardized scanning mode for sources at different locations.)

For mono-parameter δ -function distributions of p , Γ , and ℓ'_e , we have

$$\frac{d\dot{N}(>\hat{f}_\epsilon)}{d\Omega} = \frac{c}{H_0} \int_{\hat{f}_\epsilon}^{\infty} df_\epsilon \int_0^1 d\mu \int_0^{\infty} dz \frac{d_L^2(z) \dot{n}_{com}(\ell'_e, p, \Gamma; z)}{(1+z)^3 \sqrt{\Omega_m(1+z)^3 + \Omega_\Lambda}} \delta[f_\epsilon - f_\epsilon^{proc}(\ell'_e, p, \Gamma, \mu, \hat{f}_\epsilon)], \quad (11)$$

where the various parameters specifying emission properties, including W'_e , are combined into the directional power ℓ'_e .

3.2. Peak Flux and Size Distribution

The directional peak flux distribution is given by

$$\frac{d\dot{N}}{df_\epsilon d\Omega} = \frac{c}{H_0} \int_0^1 d\mu \int_0^{\infty} dz \frac{d_L^2(z) \dot{n}_{com}(\ell'_e, p, \Gamma; z)}{(1+z)^3 \sqrt{\Omega_m(1+z)^3 + \Omega_\Lambda}} \delta[f_\epsilon - f_\epsilon^{proc}(\ell'_e, p, \Gamma, \mu, f_\epsilon)]. \quad (12)$$

This leads to the solution for the z -integrated directional peak flux distribution

$$\frac{d\dot{N}}{df_\epsilon d\Omega} = \frac{c}{\beta \Gamma q H_0 f_\epsilon} \int_0^{\infty} dz \frac{d_L^2(z) \dot{n}_{com}(z) H(\mu; 0, 1)}{(1+z)^3 \sqrt{\Omega_m(1+z)^3 + \Omega_\Lambda}}, \quad (13)$$

with the Heaviside function $H(x; a, b) = 1$ when $a \leq x < b$ and $H(x; a, b) = 0$ otherwise. The cosine angle that satisfies these conditions is

$$\hat{\mu}(z, \Gamma, \ell'_e, p, q, \epsilon, f_\epsilon) = \hat{\mu} = \frac{1}{\beta} \left[1 - \frac{1}{\Gamma} \left(\frac{\ell'_e \epsilon_z^{\alpha_\nu}}{d_L^2 f_\epsilon} \right)^{1/q} \right]. \quad (14)$$

The νF_ν flux size distribution of blazars per sr per s is therefore given by

$$\frac{d\dot{N}}{d\Omega}(> f_\epsilon) = \frac{c}{H_0} \int_0^\infty dz \frac{d_L^2(z) \dot{n}_{com}(z)}{(1+z)^3 \sqrt{\Omega_m(1+z)^3 + \Omega_\Lambda}} [1 - \max(0, \hat{\mu})]. \quad (15)$$

3.3. Redshift Distribution

The directional redshift distribution above νF_ν flux f_ϵ is given by

$$\frac{d\dot{N}}{dz d\Omega}(> f_\epsilon) = \frac{c}{H_0} \frac{d_L^2(z) \dot{n}_{com}(z)}{(1+z)^3 \sqrt{\Omega_m(1+z)^3 + \Omega_\Lambda}} [1 - \max(0, \hat{\mu})]. \quad (16)$$

3.4. Setting Parameters

A γ -ray blazar can be detected from redshifts of order unity at the level f_ϵ when the parameters satisfy the condition

$$f_\epsilon \cong \frac{\Gamma^q \ell'_e (2\epsilon)^{\alpha_\nu}}{d_L^2(z=1)}, \quad (17)$$

which holds when $\Gamma \gg 1$. If a significant fraction of the DEGRB originates from blazars, then $p = 3.2$. For synchrotron or Thomson processes, this implies a photon number index $\alpha_{ph} = 2.1$, or $\alpha_\nu = -0.1$. EGRET observations of blazar spectral indices show that $\alpha_{ph} = 2.03 \pm 0.09$ for BLs and $\alpha_{ph} = 2.20 \pm 0.05$ for FSRQs, with an average spectral index of $\alpha_{ph} = 2.15 \pm 0.04$ (Mukherjee et al. 1997). The weak evidence from EGRET that α_{ph} is harder for BLs than for FSRQs is expected if, as indicated by observations, the νF_ν peaks of the synchrotron and Compton components of BLs are at higher energies than for FSRQs. Moreover, observations suggest that the flaring state spectra are harder than the quiescent emission, at least in the case of PKS 0528+134 (Mukherjee et al. 1996).

For γ -ray observations in the range $\epsilon \cong 200 - 20,000$ (i.e., 100 MeV – 10 GeV) and taking $\alpha_\nu = -0.1$, eq. (17) becomes

$$f_\epsilon \cong 10^{-11} \left(\frac{\Gamma}{10} \right)^6 \left(\frac{\ell'_e}{10^{40} \text{ ergs s}^{-1} \text{ sr}^{-1}} \right) \text{ ergs cm}^{-2} \text{ s}^{-1} \quad (18)$$

for EC statistics. For synchrotron or SSC statistics,

$$f_\epsilon \cong 10^{-11} \left(\frac{\Gamma}{10} \right)^4 \left(\frac{\ell'_e}{10^{42} \text{ ergs s}^{-1} \text{ sr}^{-1}} \right) \text{ ergs cm}^{-2} \text{ s}^{-1} \quad (19)$$

In actual fitting of blazar statistical distribution, a degeneracy between Γ and ℓ'_e is found that may be removed by obtaining limits on the bulk Lorentz factor Γ from $\gamma\gamma$ attenuation arguments (e.g. Maraschi et al. 1992; Dermer & Gehrels 1995).

For standard FSRQ blazar parameters, we take

$$p = 3.2, \Gamma = 10, \ell'_e = 10^{40} \text{ ergs s}^{-1} \text{ sr}^{-1}, \text{ BFR 3, and EC statistics.} \quad (20)$$

Note that ℓ'_e is set by a single parameter, but combines a number of physical properties besides the energy W'_e in nonthermal electrons, for example, the mean magnetic field, the emitting region size, and the properties of the external radiation field.

On Ms observing periods, EGRET saw ≈ 50 flaring blazars above its threshold νF_ν flux $f_\epsilon^{thr2} \cong 10^{-11}$ ergs $\text{cm}^{-1} \text{s}^{-1}$ at a rate $\approx 4 \text{ sr}^{-1} \text{ Ms}^{-1}$, implying a fiducial rate density $\dot{n}_{com}(z = 1)$ at redshift unity of about

$$4 \times 10^{-6} \cong \frac{c}{H_0} 4 \times 10^{56} d_{z=1}^2 \dot{n}_{com}(z = 1), \quad (21)$$

so that $\dot{n}_{com} \cong 0.8 \times 10^{-90}$ events $\text{cm}^{-3} \text{s}^{-1}$. We take $\dot{n}_{com} = 10^{-90}$ events $\text{cm}^{-3} \text{s}^{-1}$ in the calculations. The discrepancy between the calculations using this source density and the EGRET detection rate can be traced back to several factors: an additional increase of $\dot{n}_{com}(z = 1)/\dot{n}_{com}(z = 0)$ by as much as two orders of magnitude from the BFR, a reduction in the detection rate by $\approx 1/\Gamma^2$, representing the ratio of the opening angle of a two-sided jet source to 4π , and an event-rate reduction due to cosmological effects.

3.5. Blazar Formation Rate Histories

The comoving density of blazar sources or rate densities of blazar flares are assumed to follow one of 4 behaviors:

1. Constant comoving rate k , with k adjusted to make the rate density of bursting sources agree with EGRET blazar flare observations. This form is employed for mathematical convenience.
2. Comoving rate \propto the blue/UV luminosity density, which is assumed to track the star formation rate (SFR) history of the universe. We use the analytic form (Wick et al. 2004)

$$SFR = \frac{1 + a_1}{(1 + z)^{-a_2} + a_1(1 + z)^{a_3}}, \quad (22)$$

with $a_1 = 0.005$, $a_2 = 3.3$, $a_3 = 3.0$. Blazar activity could be related to the SFR if stellar activity provides fuel for the supermassive black hole engine, for example, from material driven off by starburst nurseries encircling the nucleus.

3. Comoving rate evolving with SFR, including extreme corrections (Blain et al. 1999) for dust absorption. This rate is given by Eq. (22), but with $a_1 = 0.0001$, $a_2 = 4$, $a_3 = 3$. Hopkins & Beacom (2006) give a recent review of the SFR data, and derive a SFR history that is intermediate between BFR 2 and 3, with a peak redshift at $\approx 2.5 - 3$.
4. Comoving rate \propto sub-mm/far-IR luminosity density associated with luminous IR galaxies (Sanders 2004), with the analytic form

$$\dot{n}_{com}(z) \text{ or } n_{com} \propto \left[\frac{1}{(1 + z)^8} + \frac{1}{256} \right]^{-1}. \quad (23)$$

If IR-luminous galaxies are caused by galactic merger events, as is generally argued from the morphological and spectral evidence (e.g., Sanders & Mirabel 1996, and references therein), this would connect blazars and the formation of supermassive black holes to galaxy collisions.

Fig. 3 shows the analytic forms of the BFR functions considered here.

3.6. Diffuse Intensity

The apparently diffuse intensity from the superposition of emissions from many faint, unresolved blazars is given by

$$\epsilon I_\epsilon = \frac{c}{4\pi H_0} \int_0^\infty dz \oint d\Omega_* \frac{\epsilon_*^2 q_{com}(\epsilon_*, \Omega_*; z)}{(1+z)^3 \sqrt{\Omega_m(1+z)^3 + \Omega_\Lambda}} \quad (24)$$

for persistent blazar sources. The comoving emissivity of these sources is

$$\epsilon_*^2 q_{com}(\epsilon_*, \Omega_*; z) = \frac{dE_\gamma}{dt_* dV_{com} d\Omega_*} = n_{com}(z) \ell'_e \delta_D^q \epsilon_z^{\alpha_\nu}. \quad (25)$$

When sources are detected above flux f_ϵ , they no longer contribute to the DIGBR. This restricts eq. (24) to only those blazars with $\ell'_e \delta_D^q \epsilon_z^{\alpha_\nu} / d_L^2 < f_\epsilon$, leading to the following expression for the diffuse radiation from unresolved radio galaxies and black hole jet sources:

$$\epsilon I_\epsilon^{bl} (< f_\epsilon) \cong \frac{c \ell'_{proc} \epsilon^{\alpha_\nu}}{(q-1) H_0 \beta \Gamma^q} \int_0^\infty dz \frac{(1+z)^{\alpha_\nu-3} n_{com}(z)}{\sqrt{\Omega_m(1+z)^3 + \Omega_\Lambda}} \{[1 - \beta \min(1, \hat{\mu})]^{1-q} - 1\}, \quad (26)$$

with no contribution to the integral when $\hat{\mu} \leq 0$.

From eq. (24), the diffuse intensity from blazars can be estimated as

$$\epsilon I_\epsilon (\text{ keV cm}^{-2} \text{ sr}^{-1} \text{s}^{-1}) \sim \frac{c}{H_0} \frac{\ell'_e \epsilon^{\alpha_\nu} \Gamma^{2q-2}}{1.6 \times 10^{-9} \Gamma^q} n_{com}(z \approx 1)$$

noting that the dominant contribution to emission from beamed sources occurs when $\hat{\mu} \approx \beta$. Equating the EGRET two-week average fluxes with blazars that flare once in two weeks ($\approx 10^6$ s on-source observing time) allows us to replace

$$n_{com}(z) (\text{cm}^{-3}) \cong \Delta t \dot{n}_{com}(z) \cong 10^{-84} \left(\frac{\Delta t}{10^6 \text{ s}} \right) \left[\frac{\dot{n}_{com}(z)}{10^{-90} \text{ cm}^{-3} \text{s}^{-1}} \right]$$

in the above estimate to give $\epsilon I_\epsilon \sim 4 \times 10^{-4} \text{ keV cm}^{-2} \text{sr}^{-1} \text{s}^{-1}$ times a factor that normalizes \dot{n}_{com} for a particular BFR to the measured redshift distribution of γ -ray blazars of a certain type.

The important step here is to replace the blazar density used to calculate the intensity from eq. (24) with the blazar rate density used to fit the blazar flare redshift and size distribution, using a flaring timescale of 10^6 s. The accuracy of this assumption can be answered with GLAST. Note that a selection bias may arise for detection of sources that produce frequent low-fluence flares versus sources that produce occasional high-fluence flares over a specified time interval where, in both cases, the sources are assumed to produce flares with the same peak luminosity and total apparent energy in γ rays. Because of the possible loss of detections near the EGRET blazar flux threshold, we are not very careful about fitting there.

4. Results

Calculations of observed properties are performed with the standard FSRQ blazar parameter set, eq. (20), as measured by a γ -ray telescope with EGRET detection properties given by a νF_ν threshold sensitivity of $2 \times 10^{-12} \text{ ergs cm}^{-2} \text{s}^{-1}$ at $\epsilon = 200$. Fig. 4 shows the effect of different BFRs on blazar redshift distribution. In this calculation, standard model FSRQ blazars emit blazar flares throughout the universe in random directions with a rate density that is proportional to the various z-dependent rate densities described in

Section 3.5, and a local rate density $\dot{n}_{com}(z \ll 1) = 10^{-90} \text{ cm}^{-3} \text{ s}^{-1}$. By examining Fig. 4 one sees that the redshift maxima z_{max} , namely the redshifts where the redshift distribution peaks for BFRs 1, 2, 3, and 4 are $\approx 0.5, 1, 2$, and 1.5 , respectively. These values of z_{max} correspond in cases 2, 3, and 4 to the redshifts of the maximum values of the comoving BFR rates (compare Fig. 3). From the EGRET data for FSRQs, the value of $z_{max} \approx 1$, which would favor BFR 4 and 2 over BFR 3. It will be interesting to see what GLAST finds for z_{max} for the different populations of blazars, and whether this value differs from EGRET due to different detector capabilities.

The variation of the FSRQ redshift distribution with changes in ℓ'_e , with all other parameters standard, is shown in Fig. 5. Here we use BFR 3. Increasing the comoving directional power ℓ'_e increases the maximum observable distance or redshift z_{max} until $z_{max} \approx 2.5$, corresponding to the peak value of BFR 3. It is obvious that blazars with larger ℓ'_e values are detectable from larger redshifts.

Fig. 6 shows how model redshift distributions change when Γ is changed, with all other parameters given by values for a standard FSRQ blazar. Low Γ emissions cannot be seen from large distances, as in the case for low values of ℓ'_e . The differences between the distributions where ℓ'_e and Γ change can be seen at $z \gg 1$; the large Γ blazars have small opening angle jets that reduce the detectable fraction of high-redshift blazars.

Redshift distributions for a standard FSRQ blazar with an EC beaming pattern are compared in Fig. 7 to blazars with synchrotron/SSC beaming patterns. Larger values of ℓ'_e are required for synchrotron/SSC than for EC statistics to produce similar redshift distributions when the blazars have the same Γ factors. Even when ℓ'_e or Γ is adjusted, significant differences in the redshift distribution is found for sources that obey one set of statistics or the other.

The redshift distribution of flares from a standard model FSRQ blazar for different telescope detection sensitivities f_ϵ is shown in Fig. 8. The observing frequency $\epsilon = 2000$ (≈ 1 GeV) and we use BFR 4. The two-week average EGRET sensitivity on this scale is $\approx 2 \times 10^{-11} \text{ ergs cm}^{-2} \text{ s}^{-1}$. GLAST will reach sensitivities of $f_\epsilon \approx 5 \times 10^{-13} \text{ ergs cm}^{-2} \text{ s}^{-1}$ after ≈ 3 years in the scanning mode (eq. [A23]). GLAST would see $\sim 5\%$ of blazars with $z \gtrsim 5$ at these flux values.

Blazar size distributions showing the number of blazar flares per sr per Ms exceeding νF_ν flux f_ϵ at $\epsilon = 2000$ are plotted in Fig. 9 for the standard model FSRQ with BFR 4. The size distribution of blazars that originate from maximum redshifts and from a range of redshifts, as listed in the figure caption, are plotted in the upper and lower panels, respectively. As can be seen, the brightest blazars originate at low redshifts, and good sensitivity is needed to detect high redshift blazars. For the beamed statistics, unlike Euclidean statistics, dim blazars can also originate from small redshifts. Bright blazar flares can also be detected from large redshifts when Γ or ℓ'_e is large.

5. Predictions

Illustrative results of the method applied to the EGRET sample are presented as a test case for more detailed analyses of EGRET and GLAST data. Fig. 1 shows representative fits to the redshift distributions of FSRQ and BLs. The differences between the parameters for the blazar flares used in these fits and those for the standard model FSRQ blazar is that $\Gamma = 8$ for the FSRQs rather than 10, and that $\Gamma = 5, \ell'_e = 10^{42} \text{ ergs s}^{-1} \text{ sr}^{-1}$, and synchrotron/SSC statistics are used for the BLs. The normalization factors applied to the rate density in order to fit the redshift distribution are 117 and 644 for FSRQs and BLs, respectively.

This implies a local rate density of blazar flares of

$$\dot{n}_{com}(z \ll 1) \cong 3.4 \text{ Gpc}^{-3} \text{ Ms}^{-1} \text{ for FSRQs, and } \dot{n}_{com}(z \ll 1) \cong 20 \text{ Gpc}^{-3} \text{ Ms}^{-1} \text{ for BLs.}$$

The fits tend to overproduce the number of blazars at higher redshifts, keeping in mind the prior knowledge that the EGRET observations show that there are high- z tails to the BL and FSRQ distributions. The addition of a lower Γ , ℓ'_e component would improve the fit, though at the expense of an additional set of parameters.

The predicted size distributions of FSRQs and BLs from this fit to the EGRET redshift distribution are shown by the dotted and dot-dashed curves in Fig. 2. The bolometric threshold sensitivities are $\approx 40 - 100 \times$ better for GLAST than EGRET, namely at the level of $1 - 2 \times 10^{-12} \text{ ergs cm}^{-2} \text{ s}^{-1}$ (the values of f_ϵ used in the calculation are a factor ≈ 5 smaller to account for the bolometric correction). The model fit predicts that GLAST will detect ≈ 1000 FSRQs and ≈ 5000 BLs.

The left and right panels of Fig. 10 show predicted FSRQ and BL blazar redshift distributions, respectively, for a γ -ray telescope with EGRET-like detection characteristics and one with GLAST-like characteristics. BFR 4 is assumed. The distribution predicted for EGRET is shown by the lower curves in the two panels, and the predicted distributions for GLAST sensitivities of $5 \times 10^{-13} \text{ cm}^{-2} \text{ s}^{-1}$ and $10^{-13} \text{ cm}^{-2} \text{ s}^{-1}$ are shown by the middle and upper pair of curves. The bounds on the curves are determined by the ≈ 100 MeV – 1 GeV photon energies that describe GLAST’s most sensitive energy range (see Appendix).

We have not yet, however, taken into account the constraint from the DIGRB. Fig. 11 shows the contribution to the DEGRB as reported by the EGRET team (filled data points; Sreekumar et al. 1998), and as derived from the EGRET data using the GALPROP cosmic-ray propagation code (open data points; Strong et al. 2000, 2004). The curves show calculations of the contributions to the DEGRB from unresolved FSRQs and BLs. An interesting feature of the calculation is that even though we have considered a single spectral index p , the integration in eq. (26) produces weak curvature of the diffuse background spectrum. Integrating the FSRQ contribution over all redshifts gives a contribution to the DEGRB that is a factor of 2 – 3 below the level reported by Sreekumar et al. (1998). Integrating the BL contribution over all redshifts overproduces the γ -ray background. This implies that the BL contribution at high redshifts must diminish, either due to a reduction in the number of sources or through luminosity evolution in the sources (that is, a reduction in the mean values of Γ or ℓ'_e). Also implicit here is that FSRQs and BLs follow the same BFR.

6. Discussion and Summary

We have developed a physical model to fit population statistics of EGRET γ -ray blazar data and data anticipated from GLAST. The standard model blazar used in this study has comoving directional leptonic power $\ell'_e = 10^{40} \text{ ergs s}^{-1} \text{ sr}^{-1}$, $\Gamma = 10$, and $p = 3.2$. We use the the EC beaming pattern for FSRQs, and the synchrotron/SSC beaming pattern for BLs. The basic features of the EGRET observations of the redshift and size distributions of FSRQs and BLs are reproduced with BFR 4 for standard model blazars with $\Gamma = 8$ for the FSRQs, and $\Gamma = 5$ and $\ell'_e = 10^{42} \text{ ergs s}^{-1} \text{ sr}^{-1}$ for the BLs. These values of Γ are generally consistent with Lorentz factors inferred from fits to the local luminosity function of blazars (Urry & Padovani 1995) and measurements of superluminal motions (Vermeulen & Cohen 1994). The superluminal motion observations indicate that BLs have smaller Doppler factors on average than FSRQs, though in both cases the spread in Doppler factors is rather large (Jorstad et al. 2001).

Measurements of superluminal motion and the radio luminosity function are based on radio observations

of outflowing radio-emitting plasma on the scale of $\approx 0.1 - 1$ pc from the black hole. The γ rays may originate from within hundreds to thousands of Schwarzschild radii of the supermassive black hole, so that the Γ values derived from radio observations may not be appropriate to the analysis of γ -ray data. Radio observations suggest, however, that γ -ray flares originate from the same physical scale as the superluminal blobs (Jorstad et al. 2001a), but it then becomes difficult to understand why spectral modeling of some X-ray selected BLs such as Mrk 421 and Mrk 501 give Doppler factors ≈ 50 (e.g., Krawczynski et al. 2001), much larger than the values observed in superluminal motion observations.² In any case, lower limits to the values of Γ for BLs and FSRQs will be inferred from $\gamma\gamma$ attenuation arguments applied to the GLAST observations. This will not only provide reliable values to use for modeling the population statistics of γ -ray blazars, but will help break the degeneracy in Γ and ℓ'_e in the modeling.

By fitting the EGRET data and then readjusting the detector properties for values characteristic of GLAST, we found that GLAST would observe ≈ 1000 FSRQs and ≈ 5000 BLs. The contribution of the many weak BLs would, however, overproduce the γ -ray background. Thus we conclude from the EGRET observations alone that there must be a cutoff in the high-redshift source density or reduction in source luminosities of BLs. Negative density evolution of X-ray selected BLs has been established (Wolter et al. 1994; Padovani & Giommi 1995), and it is satisfying that the same inference is obtained through γ -ray modeling. This outcome makes it, unfortunately, difficult to predict reliably the number of BLs that GLAST will observe. In future work, we plan to repeat the analysis with a larger EGRET data set that has the BLs separated into radio-selected BLs and X-ray selected BLs, and consider luminosity evolution due to the growth of black holes through cosmic time. This will test evolutionary scenarios where the FSRQs evolve into BLs (Böttcher & Dermer 2002; Cavaliere & D'Elia 2002).

Fits to the EGRET γ -ray data are best with BFR 4, corresponding to a cosmic evolution of blazar rate densities proportional to the far IR/sub-millimeter luminosity density inferred from observations of IR luminous galaxies (Sanders 2004). An important feature of this BFR is a rate reduction at $z \approx 1$ that reproduces the peak redshift near unity of the EGRET FSRQ redshift distribution. The better statistics from GLAST will show whether this peak redshift is a feature of the cosmic evolution of blazars. The IR radiation from hot dust in the vicinity of the central nucleus provides another target photon source (e.g., Błażejowski et al. 2000) that affects the spectral properties of blazars, so population and spectral evolution should be treated jointly.

The purpose of this work is to outline a method to analyze the population statistics of γ -ray blazars solely from the γ -ray data. There is, of course, a close connection between the radio and γ -ray properties of blazars that makes it possible to perform statistical studies that invoke a radio/ γ -ray connection (see Introduction). Performing the γ -ray population study independent of other wavebands will allow us to check the reliability of that method, and to explore the physical reasons for differences in radio galaxy and blazar populations selected from observations at different wavebands.

I thank Stanley P. Davis for helping assemble the sample used in the analysis, and Truong Le for discussions. I would also like to thank J. Chiang, S. Ciprini, B. Dingus, P. Giommi, J. McEnery, G. Madejski, A. Reimer, and R. Romani for useful comments and discussions that influenced this work. Thanks are also due to B. Lott and P. Michelson for encouragement, and to P. Sreekumar for providing the EGRET data for the diffuse γ -ray background. The work of C. D. D. is supported by the Office of Naval Research and GLAST Interdisciplinary Science Investigator grant DPR S-13756G.

²See Georganopoulos & Kazanas (2003) and Ghisellini et al. (2005) for proposed solutions to this puzzle.

A. Sensitivity of EGRET and GLAST to Blazar Flares

We follow the approach of Dermer & Dingus (2003). The properties of a γ -ray imaging spark chamber or silicon tracker detector depends on its shower pattern, assumed to be described by a Gaussian with 68% containment angle $\hat{\theta}$ and energy-dependent angular point spread function (psf) described by

$$\theta_{psf} = \hat{\theta} u^{-w} , \quad (\text{A1})$$

where the photon energy in units of 100 MeV is

$$u = \frac{E}{E_{100}} \text{ and } E_{100} = 100 \text{ MeV} . \quad (\text{A2})$$

For EGRET, $\hat{\theta} \cong 5.7^\circ/57.3^\circ \cong 0.1$ and $w = 1/2$. For GLAST, $\hat{\theta} \cong 3.5^\circ/57.3^\circ \cong 0.06$ and $w = 2/3$.

The effective area $A(E, \theta, \phi)$ depends on photon energy E , angle θ from zenith, and azimuthal angle ϕ measured with respect to the zenith angle, according to

$$A(E, \theta, \phi) \cong A(u) \cong A_0 u_0^a , \quad (\text{A3})$$

where A_0 is the effective area averaged over the field of view, defined as the opening solid angle within which the effective area is 50% of the on-axis FOV. The FOV of EGRET is $\cong 4\pi/24 \cong 0.5$ sr, and the FOV of GLAST is $\cong 4\pi/6 \cong 2$ sr. The parameters describing the effective area A_0 at 100 MeV and index a_0 are, respectively, $\cong 1200 \text{ cm}^2$ and $a_0 \cong 0$ for EGRET, and $\cong 6200 \text{ cm}^2$ and $a_0 \cong 0.16$ for GLAST.³

The significance to detect a signal at the $n\sigma$ level is given by

$$n \cong \frac{S}{\sqrt{\alpha S + (1 + \alpha)B}} \quad (\text{A4})$$

(Li & Ma 1983, eq. 9), where S is the number of source counts, B is the number of background counts, and $\alpha = t_{on}/t_{off}$ is the ratio of on-source to off-source observing times. If the background is precisely known, $\alpha \rightarrow 0$, and

$$n \cong \frac{S}{\sqrt{B}} . \quad (\text{A5})$$

In the limit $\alpha \ll 1$ and $n \gg 1$, eqs. (1) and (2) overestimate the fluctuation probability compared to a maximum likelihood expression confirmed by Monte Carlo simulations (Li & Ma 1983), so eq. (A5) should be a conservative expression for the detection significance.

A.1. Background Counts

We assume that the source location is precisely known. The number of background photons within solid element $\Delta\Omega(E)$ centered in the direction $\vec{\Omega}$, and with energies $> E_1$ observed during an observing time Δt is

$$B(> E_1) \cong \int_0^{\Delta t} dt \int_{E_1}^{\infty} dE \Delta\Omega(E) A[E, \theta(t), \phi(t)] \Phi_B(E, \vec{\Omega}) . \quad (\text{A6})$$

³These satisfy the GLAST Science Requirements Document; the actual performance is given at the GLAST websites. Note that the estimate requires an average over the FOV.

The background photon flux per steradian, $\Phi_B(E, \vec{\Omega}) = dN_\gamma/dAdtd\Omega dE$, is assumed to be time-independent; thus this treatment excludes passage through the South Atlantic Anomaly. This expression also applies to time-independent diffuse backgrounds, not time-variable point sources or variable backgrounds. The effective area $A[E, \theta(t), \phi(t)]$ of the telescope at energy E changes for a source at time-varying angles θ and ϕ with respect to the telescope \hat{z} -axis, which change with time due to rocking or slewing or Earth occultation. These effects are taken into account with an exposure factor X . Note that eq. (A6) assumes that each photon count can be precisely assigned an energy E and direction (θ, ϕ) .

The DIGRB radiation spectrum is independent of $\vec{\Omega}$ and is given by Sreekumar et al. (1998) as

$$\Phi_X(E) = k_x u^{-\alpha_B} , \quad (A7)$$

where $k_x = 1.73 \pm 0.08 \times 10^{-7}$ ph (cm²-s-sr-MeV)⁻¹ and $\alpha_B = 2.10 \pm 0.03$. This expression is valid description for a background emission component regardless of whether the DIGRB is extragalactic (DE-GRB), or contains a quasi-isotropic high-latitude galactic emission component from cosmic ray electrons that Compton-scatter the ambient CMB, IR and stellar radiation fields (Strong et al. 2004). The galactic diffuse flux is ~ 9 and ~ 29 times brighter than the extragalactic diffuse flux in the inner Galaxy region at 100 MeV and 1 GeV, respectively (see Hunter et al. 1997, for spectra of diffuse galactic flux). Thus the number of background counts with energy E observed over the real time $\Delta t = t_{wk}$ weeks is

$$B(> u) = \frac{X \Delta t E_{100} \pi \hat{\theta}^2 A_0 k_x}{2w + \alpha_B - 1 - a_0} u^{1+a_0-2w-\alpha_B} , \quad (A8)$$

A.2. Source Counts

For a point source, the number of source counts with energy $> E$ is given by

$$S(> E_1) \cong f_\gamma \int_0^{\Delta t} dt \int_{E_1}^{\infty} dE A[E, \theta(t), \phi(t)] \phi_s(E, t) , \quad (A9)$$

where $\phi_s(E, t)$ is the source photon flux (ph cm⁻² s⁻¹ E⁻¹) and we assume that the point spread function is defined as the $f_\gamma = 68\%$ containment radius (see Thompson 1986). Thus

$$S(> u) \cong \frac{10^{-8} f_\gamma X_s \Delta t (\alpha_{ph} - 1) A_0 \phi_{-8}}{\alpha_{ph} - a_0 - 1} u^{1+a_0-\alpha_{ph}} , \quad (A10)$$

and α_{ph} is the photon number index (commonly denoted Γ). The factor X_s accounts for the on-source exposure, and is generally equal to the background exposure factor X , though it may differ if one allows X_s to account for the source duty cycle, or if X accounts for variable background. The quantity ϕ_{-8} normalizes the source flux

$$\phi_s(E) = \frac{10^{-8} (\alpha_{ph} - 1) \phi_{-8}}{E_{100}} u^{-\alpha_{ph}} \quad (A11)$$

to 10^{-8} ph($E > 100$ MeV) cm⁻² s⁻¹, which is the unit quoted by the EGRET team in the Third EGRET catalog (Hartman et al. 1999) for the two-week average fluxes.

For EGRET, $S(> u) \cong 4.9 u^{-1.1} \phi_{-8} t_{wk} \geq 5 n_{5s}$, where a source detection is assumed to require at least 5 counts ($n_{5s} = 1$). From the signal limit, a minimum time

$$t_{wk}^E \gtrsim \frac{u^{\alpha_{ph}-1}}{\phi_{-8} X_s} n_5 \cong \frac{2u^{1.1}}{\phi_{-8}} , \quad (A12)$$

is needed for EGRET to detect sources in the EGRET FOV as faint as ϕ_{-8} (assuming that the blazar remains at the level of ϕ_{-8} during the entire viewing period). Earth occultation means $X_s \approx 1/2$. The final expression in eq. (A12) applies when $\alpha_{ph} = 2.1$, the index of the isotropic γ -ray background. Here we suppose that blazars make a large fraction of the DEGRB, and so must have a significant fraction of bright blazar sources emitting with $\alpha_{ph} \cong 2.3$ between ≈ 100 MeV and 10 GeV.

For GLAST in the scanning mode, the condition for the detection of 5 counts is

$$t_{wk}^G \gtrsim \left(\frac{\alpha_{ph} - 1.16}{\alpha_{ph} - 1} \right) \frac{u^{\alpha_{ph}-1.16}}{X_{1/5}\phi_{-8}} n_{5s} \cong 0.85 \frac{u^{0.94}}{\phi_{-8}}, \quad (\text{A13})$$

where we have adopted a source occultation factor $X_s = 0.2X_{1/5}$. The two estimates are similar at 100 MeV, because the factor 6 – 8 effective area advantage of GLAST over EGRET is reduced by GLAST in the scanning mode compared with the few occasions when the source is a pointing target for EGRET.

A.3. Signal to Noise

From eqs. (A5), (A8) and (A10), the significance to detect a blazar at the $n\sigma$ level is

$$n(>u) = \frac{S(>u)}{\sqrt{B(>u)}} = \frac{10^{-8} f_\gamma X_s \sqrt{A_0 \Delta t} \phi_{-8}}{\sqrt{X \pi k_x E_{100}} \hat{\theta}} \varphi_c u^{\varphi_x}, \quad (\text{A14})$$

where

$$\varphi_c = \frac{(\alpha_{ph} - 1)}{\alpha_{ph} - a_0 - 1} \sqrt{2w + \alpha_B - 1 - a_0}, \quad (\text{A15})$$

and

$$\varphi_x = w - \alpha_{ph} + \frac{1 + a_0 + \alpha_B}{2}. \quad (\text{A16})$$

The energy dependence of the background-limited detections of blazars is defined by the index

$$\varphi_x \cong \begin{cases} 2.05 - \alpha_{ph}, & \text{EGRET} \\ 2.30 - \alpha_{ph}, & \text{GLAST} \end{cases}, \quad (\text{A17})$$

and it is of interest that EGRET and GLAST are more sensitive to hard-spectrum blazars ($\alpha_{ph} \lesssim 2 - 2.3$) at higher photon energies. This sensitivity improves until either there is a spectral break or softening, or the signal runs out.

The background limit on EGRET, with $X = X_s$, is

$$n^E(>u) = 0.36 \sqrt{X t_{wk}} \phi_{-8} u^{2.05 - \alpha_{ph}} > 5n_{5\sigma}. \quad (\text{A18})$$

Taking $X = 0.5$, due to Earth occultation, the number of weeks of direct pointing required for EGRET to detect a source with flux at the level ϕ_{-8} at the $5n_{5\sigma}\sigma$ significance level is

$$t_{wk}^E \gtrsim \frac{386}{\phi_{-8}^2} u^{2(\alpha_{ph}-2.05)} n_{5\sigma}^2. \quad (\text{A19})$$

Comparison with eq. (A12) shows, as is well known, that signal detection with EGRET is background rather than signal limited. For $u = 1$, as used in the analysis reported in the EGRET catalogs, the limiting sensitivity to detect a strong source in a two-week pointing is

$$\phi_{-8} \gtrsim 14.$$

This estimate agrees well with detection data, as seen from Fig. 2.

For GLAST, the background limit translates into the condition

$$\phi_{-8} \gtrsim \frac{3.6n_{5\sigma}}{\sqrt{X}t_{wk}} u^{\alpha_{ph}-2.3}, \quad (\text{A20})$$

so that the number of weeks of scanning required for GLAST to detect a source with flux level ϕ_{-8} at the $5n_{5\sigma}\sigma$ significance level is

$$t_{wk}^G \gtrsim \frac{64u^{2(\alpha_{ph}-2.3)}n_{5\sigma}^2}{X_{1/5}\phi_{-8}^2} \rightarrow \frac{64}{\phi_{-8}^2} u^{-2/5}. \quad (\text{A21})$$

Thus, in around a year in the scanning mode, GLAST will detect sources at the level $\phi_{-8} \sim 1$ when integrating above 100 MeV ($u = 1$). This is not however the best detection strategy.

A.4. Optimal Source Detection with GLAST

A better analysis considers optimal energy for source detection from both signal and noise limits. Equating eqs. (A13) and (A21) for the minimum time needed to detect sources at the 5σ , 5 count limit assuming $p = 3.2$ or $\alpha_\nu = -0.1$, gives the best lower photon energy above which to integrate, namely

$$\bar{u} \cong 20 \phi_{-8}^{-3/4}, \text{ or } \bar{E} \cong 2.0\phi_{-8}^{-3/4} \text{ GeV}. \quad (\text{A22})$$

The time it takes to reach this flux level is

$$\bar{t}_{wk} \cong \frac{14}{\phi_{-8}^{1.7}}. \quad (\text{A23})$$

Fig. 12 shows the minimum time for GLAST to detect sources at different integral flux levels ϕ_{-8} and with different spectral indices from the signal and background limits, eqs. (A13) and (A21), respectively. In order to determine the source's spectral index, a hardness ratio or mean photon energy $\langle E \rangle$ can be calculated for photons originating from a source at a known source position. For photons with energies between 100 MeV and $E_2 = 100u_2$ MeV originating from a source with spectral index α_{ph} ,

$$\langle E \rangle = E_{100} \left(\frac{\alpha_{ph} - 1 - a_0}{\alpha_{ph} - 2 - a_0} \right) \frac{1 - u_2^{\alpha_{ph}-2-a_0}}{1 - u_2^{\alpha_{ph}-1-a_0}}. \quad (\text{A24})$$

Background contamination must also be considered to determine the best value and error for α_{ph} . The upper energy used for u_2 depends on the nature of the source spectrum or the cutoff produced by $\gamma\gamma$ attenuation on the EBL. For low redshift sources, contemporaneous observations with MAGIC, HESS, or VERITAS ground-based γ -ray telescopes could help constrain the upper energy. Higher energy analysis can enhance blazar detection. For example, Dingus & Bertsch (2001) reported the search for blazars in the EGRET data by looking at > 10 GeV photons.

A.5. Short Timescale Flares

GLAST reaches EGRET 2-week sensitivities of $\phi_{-8} \cong 15$ after $\approx 1 - 2$ days, as can be obtained by comparing eq. (A23) with eq. (A21). It reaches this sensitivity over the *full sky*, compared to $\approx 1/24^{\text{th}}$ of the full sky viewed with EGRET. For a mean photon energy of ≈ 400 MeV measured with EGRET from

a blazar with $2 \lesssim \alpha_{ph} \lesssim 2.5$, a measurement of $\phi_{-8} \cong 15$ (150) corresponds to an energy flux between 100 MeV and 5 GeV of $\cong 10^{-10}$ (10^{-9}) ergs cm $^{-2}$ s $^{-1}$.

Consider a flare at the level of $\phi_{-8} \cong 200$, corresponding to some of the brightest flares seen with EGRET. Given the Phase 1 EGRET all-sky survey results (Dermer & Dingus 2003), we predict a flare at this level every few days, with large uncertainties given the small statistics of bright blazar flares. For a blazar with γ -ray spectral index $\alpha_{ph} = 2.1$, GLAST will have a significant 5σ detection after

$$\bar{t} \cong 2.6 \text{ ks} , \quad (\text{A25})$$

using $\bar{u} = 1$ whenever $\bar{u} < 1$. Better sensitivity of a bright blazar flare is possible for observing times less than the GLAST orbital period of 1.6 hr (or 5.8 ks) if the blazar is in the FOV of GLAST. In this case, X_s can be larger than 1/5. These timescales are of particular interest inasmuch as we expect a minimum variability timescale t_{var} corresponding to a light-crossing distance

$$t_{var} = \frac{2GM}{c^3} (1+z) \approx M_8(1+z) \text{ ks} ; \quad (\text{A26})$$

corrections should be made to this expression for a Kerr metric. Temporal power analyses of strings of data from bright blazars, such as 3C 279 and PKS 0528+134, could find a reduction of power at a timescale corresponding to the Schwarzschild radius or radius of the minimum stable orbit. Rare, bright, hard spectrum flares are of particular interest for GLAST analysis in order to look for $\gamma\gamma$ absorption cutoffs, whether internal (within the blob), external within the inner jet or galactic environment, or due to absorption on diffuse radiation fields.

REFERENCES

Blain, A. W., Jameson, A., Smail, I., Longair, M. S., Kneib, J.-P., & Ivison, R. J. 1999, MNRAS, 309, 715
 Błażejowski, M., Sikora, M., Moderski, R., & Madejski, G. M. 2000, ApJ, 545, 107
 Böttcher, M., & Dermer, C. D. 2002, ApJ, 564, 86
 Cavaliere, A., & D'Elia, V. 2002, ApJ, 571, 226
 Chiang, J., Fichtel, C. E., von Montigny, C., Nolan, P. L., & Petrosian, V. 1995, ApJ, 452, 156; (e) 1996, ApJ, 465, 1011
 Chiang, J., and Mukherjee, R. 1998, ApJ, 496, 752
 Dermer, C. D., & Dingus, B. L. 2003, New Astronomy Rev., 48, 537
 Dermer, C. D., & Schlickeiser, R. 2002, ApJ, 575, 667
 Dermer, C. D., & Davis, S. P. 2000, in the Fifth Compton Symposium (AIP: New York), ed. M. L. McConnell & J. M. Ryan, 510, 425
 Dermer, C. D., Sturner, S. J., & Schlickeiser, R. 1997, ApJS, 109, 103
 Dermer, C. D., and Gehrels, N. 1995, ApJ, 447, 103; (e) 1996, ApJ, 456, 412
 Dermer, C. D. 1995, ApJ, 446, L63

Dermer, C. D. 1992, Phys. Rev. Lett., 68, 1799

Dingus, B. L., & Bertsch, D. L. 2001, AIP Conf. Proc. 587: Gamma 2001: Gamma-Ray Astrophysics, 587, 251

Fichtel, C. E., et al. 1994, ApJS, 94, 551

Georganopoulos, M., Kirk, J. G., & Mastichiadis, A. 2001, ApJ, 604, 479; (e) 2001, ApJ, 561, 111

Georganopoulos, M., & Kazanas, D. 2003, ApJ, 594, L27

Ghisellini, G., Tavecchio, F., & Chiaberge, M. 2005, A&A, 432, 401

Giommi, P., Colafrancesco, S., Cavazzuti, E., Perri, M., & Pittori, C. 2006, A&A, 445, 843

Gould, R. J. 1979, A&A, 76, 306

Hartman, R. C. et al. 1999, ApJS, 123, 79

Hopkins, A. W., & Beacom, J. F. 2006, ApJ, submitted (astro-ph/0601463)

Hunter, S. D., Kinzer, R. L., and Strong, A. W., 1997, in the Fourth Compton Symposium, ed. C. Dermer, M. Strickman, and J. Kurfess (AIP: New York), p. 192

Jorstad, S. G., Marscher, A. P., Mattox, J. R., Wehrle, A. E., Bloom, S. D., & Yurchenko, A. V. 2001, ApJS, 134, 181

Jorstad, S. G., Marscher, A. P., Mattox, J. R., Aller, M. F., Aller, H. D., Wehrle, A. E., & Bloom, S. D. 2001a, ApJ, 556, 738

Krawczynski, H., et al. 2001, ApJ, 559, 187

Kühr, H., Witzel, A., Pauliny-Toth, I. I. K., & Nauber, U. 1981, A&AS, 45, 367

Li, P.-P., & Ma, Y.-Q. 1983, ApJ, 272, 317

Lind, K. R., & Blandford, R. D. 1985, ApJ, 295, 358

Maraschi, L., Ghisellini, G., & Celotti, A. 1992, ApJ, 397, L5

Maraschi, L., & Tavecchio, F. 2003, ApJ, 593, 667

Mücke, A., & Pohl, M. 2000, MNRAS, 312, 177

Mukherjee, R., et al. 1996, ApJ, 470, 831

Mukherjee, R., et al. 1997, ApJ, 490, 116

Narumoto, T., & Totani, T. 2006, ApJ, submitted (astro-ph/0602178)

Perlman, E. S., et al. 1996, ApJS, 104, 251

Padovani, P. and Giommi, P. 1995, MNRAS, 277, 1477

Padovani, P. and Giommi, P. 1995a, ApJ, 444, 567

Romani, R. W., Sowards-Emmerd, D., Greenhill, L., & Michelson, P. 2004, ApJ, 610, L9

Sanders, D. B., & Mirabel, I. F. 1996, *ARA&A*, 34, 749

Sanders, D. B. 2004, *Advances in Space Research*, 34, 535

Sikora, M., Madejski, G., Moderski, R., & Poutanen, J. 1997, *ApJ*, 484, 108

Sowards-Emmerd, D., Romani, R. W., Michelson, P. F., Healey, S. E., & Nolan, P. L. 2005, *ApJ*, 626, 95

Spergel, D. N., et al. 2003, *ApJS*, 148, 175

Sreekumar, P., et al. 1998, *ApJ*, 494, 523

Stawarz, L., Kneiske, T. M., & Kataoka, J. 2006, *ApJ*, 637, 693

Stecker, F. W., & Salamon, M. H. 1996, *ApJ*, 464, 600

Strong, A. W., Moskalenko, I. V., & Reimer, O. 2000, *ApJ*, 537, 763; (e) 2000, *ApJ*, 541, 1109

Strong, A. W., Moskalenko, I. V., & Reimer, O. 2004, *ApJ*, 613, 956

Thompson, D. J., 1986, *Nuclear Instruments and Methods in Physics Research*, A251, 390

Urry, C. M., and Padovani, P. 1995, *PASP*, 107, 803

Vermeulen, R. C., & Cohen, M. H. 1994, *ApJ*, 430, 467

Wolter, A., Caccianiga, A., della Ceca, R., & Maccacaro, T. 1994, *ApJ*, 433, 29

Wick, S. D., Dermer, C. D., & Atoyan, A. 2004, *Astroparticle Physics*, 21, 125

Table 1: Sample of High-Confidence Gamma-Ray Blazars used in Analysis

| Catalog Name | ϕ_{-8}^{pk} ^a | $\Delta\phi_{-8}^{pk}$ | Redshift z | Other Name ^b | Classification ^c |
|----------------|-------------------------------|------------------------|--------------|-------------------------|-----------------------------|
| 3EG J0204+1458 | 52.8 | 26.4 | 0.405 | PKS 0202+14 | |
| 3EG J0210-5055 | 134.1 | 24.9 | 1.003 | PKS 0208-512 | |
| 3EG J0222+4253 | 25.3 | 5.80 | 0.444 | 3C 66A | B |
| 3EG J0237+1635 | 65.1 | 8.80 | 0.940 | AO 0235+164 | B |
| 3EG J0340-0201 | 177.6 | 36.6 | 0.852 | PKS 0336-01 | |
| 3EG J0412-1853 | 49.5 | 16.1 | 1.536 | PKS 0414-189 | |
| 3EG J0422-0102 | 64.2 | 34.2 | 0.915 | PKS 0420-01 | |
| 3EG J0442-0033 | 85.9 | 12.0 | 0.844 | NRAO 190 | |
| 3EG J0450+1105 | 109.5 | 19.4 | 1.207 | PKS 0446+112 | |
| 3EG J0456-2338 | 14.7 | 4.20 | 1.009 | PKS 0454-234 | |
| 3EG J0458-4635 | 22.8 | 7.40 | 0.8580 | PKS 0454-46 | |
| 3EG J0459+0544 | 34.0 | 18.0 | 1.106 | PKS 0459+060 | |
| 3EG J0500-0159 | 68.2 | 41.3 | 2.286 | PKS 0458-02 | |
| 3EG J0530+1323 | 351.4 | 36.8 | 2.060 | PKS 0528+134 | |
| 3EG J0540-4402 | 91.1 | 14.6 | 0.894 | PKS 0537-441 | B |
| 3EG J0721+7120 | 45.7 | 11.1 | 0.30 | S5 0716+714 | B |
| 3EG J0737+1721 | 29.3 | 9.90 | 0.424 | PKS 0735+178 | B |
| 3EG J0743+5447 | 42.1 | 8.30 | 0.723 | RX J0742.6+5444 | |
| 3EG J0828+0508 | 35.5 | 16.3 | 0.180 | PKS 0829+046 | B |
| 3EG J0829+2413 | 111.0 | 60.1 | 0.939 | OJ 248 | |
| 3EG J0845+7049 | 33.4 | 9.00 | 2.172 | 4C 71.07 | |
| 3EG J0852-1216 | 44.4 | 11.6 | 0.566 | PMN J0850-1213 | |
| 3EG J0853+1941 | 15.8 | 6.90 | 0.306 | OJ 287 | B |
| 3EG J0952+5501 | 47.2 | 15.5 | 0.901 | OK 591 | |
| 3EG J0958+6533 | 18.0 | 9.40 | 0.368 | S4 0954+65 | B |
| 3EG J1104+3809 | 27.1 | 6.90 | 0.031 | Mkn 421 | B |
| 3EG J1200+2847 | 163.2 | 40.7 | 0.729 | TON 0599 | |
| 3EG J1222+2841 | 53.6 | 14.1 | 0.102 | W Comae | B |
| 3EG J1224+2118 | 48.1 | 15.3 | 0.435 | PG 1222+216 | |
| 3EG J1229+0210 | 48.3 | 11.3 | 0.158 | 3C 273 | |
| 3EG J1230-0247 | 15.5 | 4.10 | 1.045 | PKS 1229-02 | |
| 3EG J1246-0651 | 44.1 | 29.6 | 1.286 | PKS 1243-072 | |
| 3EG J1255-0549 | 267.3 | 10.7 | 0.538 | 3C 279 | |
| 3EG J1329+1708 | 33.1 | 19.3 | 2.084 | OP 151 | |
| 3EG J1339-1419 | 20.2 | 11.6 | 0.539 | PKS 1335-127 | |
| 3EG J1409-0745 | 128.4 | 23.4 | 1.494 | PKS 1406-076 | |
| 3EG J1429-4217 | 55.3 | 16.3 | 1.522 | PKS 1424-41 | |
| 3EG J1512-0849 | 49.4 | 18.3 | 0.361 | PKS 1510-08 | |
| 3EG J1605+1553 | 42.0 | 12.3 | 0.357 | 4C 15.54 | B |
| 3EG J1608+1055 | 62.4 | 13.0 | 1.226 | OS 111 | |
| 3EG J1614+3424 | 68.9 | 15.3 | 1.401 | OS 319 | |
| 3EG J1625-2955 | 258.9 | 15.3 | 0.815 | PKS 1622-29 | |
| 3EG J1626-2519 | 82.5 | 35.0 | 0.786 | PKS 1622-253 | |

Table 1: (cont.) Sample of High-Confidence Gamma-Ray Blazars Used in Analysis

| Catalog Name | ϕ_{-8}^{pk} | $\Delta\phi_{-8}^{pk}$ | Redshift z | Other Name ^b | Classification ^c |
|----------------|------------------|------------------------|--------------|-------------------------|-----------------------------|
| 3EG J1635+3813 | 107.5 | 9.60 | 1.814 | 4C 38.41 | |
| 3EG J1727+0429 | 30.2 | 18.8 | 0.296 | PKS 1725+044 | |
| 3EG J1733-1313 | 104.8 | 34.7 | 0.902 | PKS 1730-13 | |
| 3EG J1738+5203 | 44.9 | 26.9 | 1.375 | OT 566 | |
| 3EG J1744-0310 | 48.7 | 19.6 | 1.054 | PKS 1741-03 | |
| 3EG J1935-4022 | 93.9 | 31.4 | 0.966 | PKS 1933-400 | |
| 3EG J1937-1529 | 55.0 | 18.6 | 1.657 | PKS 1936-15 | |
| 3EG J2025-0744 | 74.5 | 13.4 | 1.388 | PKS 2023-07 | |
| 3EG J2036+1132 | 35.9 | 15.0 | 0.601 | TXS 2032+117 | B |
| 3EG J2055-4716 | 35.0 | 20.9 | 1.489 | PKS 2052-47 | |
| 3EG J2158-3023 | 30.4 | 7.70 | 0.116 | PKS 2155-304 | B |
| 3EG J2202+4217 | 39.9 | 11.6 | 0.069 | BL Lac | B |
| 3EG J2232+1147 | 51.6 | 15.0 | 1.037 | CTA 102 | |
| 3EG J2254+1601 | 116.1 | 18.4 | 0.859 | 3C 454.3 | |
| 3EG J2321-0328 | 38.2 | 10.1 | 1.411 | PKS 2320-035 | |
| 3EG J2358+4604 | 42.8 | 20.3 | 1.992 | OZ 486 | |
| 3EG J2359+2041 | 26.3 | 9.00 | 1.066 | OZ 193 | |

^a ϕ_{-8}^{pk} : peak flux ($E > 100$ MeV) in units of 10^{-8} photons $\text{cm}^{-2} \text{ s}^{-1}$.

^bSurvey catalogs includ PKS: Parkes, O(A-Z): Ohio, 3C/4C: Cambridge, and TXS: Texas.

^cB: BL Lac object; no entry: FSRQ.

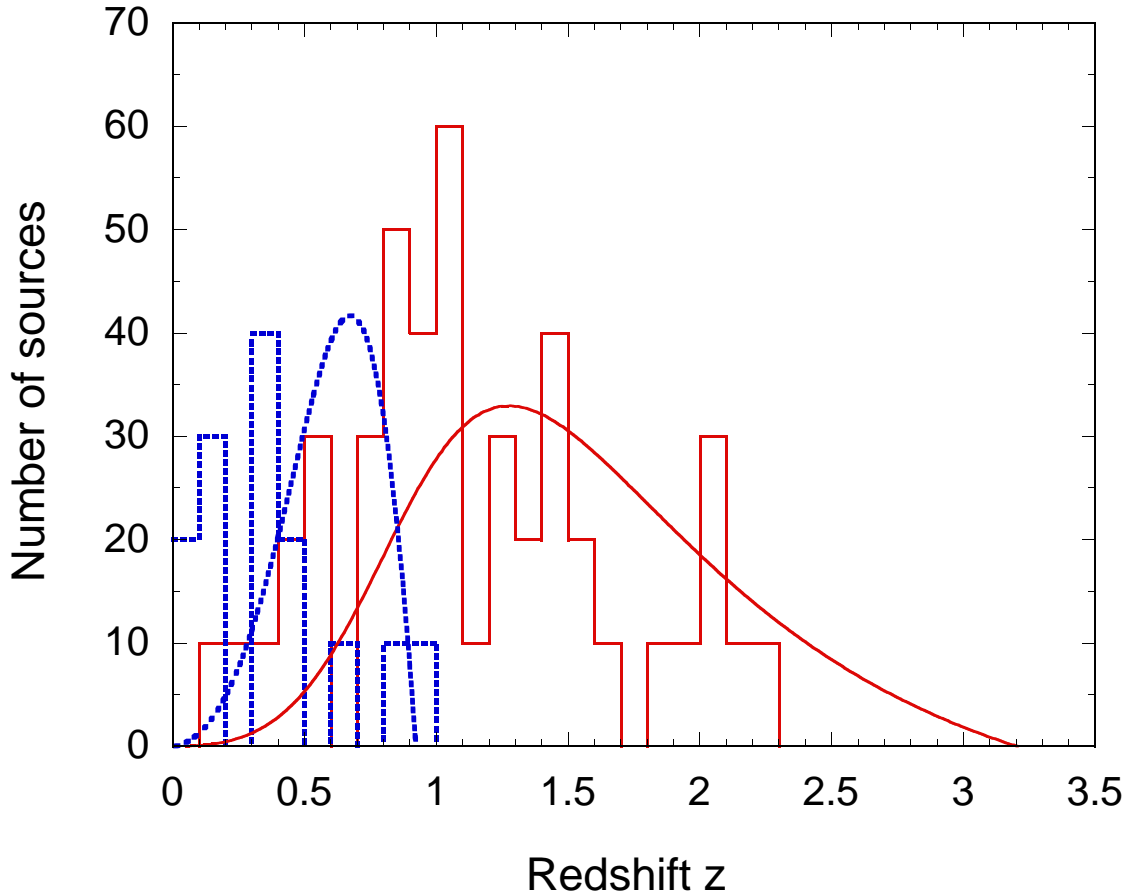


Fig. 1.— EGRET observations of the redshift distributions of blazars, separated into FSRQ (solid) and BL Lac (dotted) populations, are shown by the histograms. Smooth solid curve shows a monoparametric FSRQ blazar fit with BFR 4 (see Fig. 3), $\Gamma = 8$, EC statistics, $\ell'_e = 10^{40}$ ergs s^{-1} sr $^{-1}$, and $p = 2.3$. The dotted curve shows the monoparametric blazar fit for the BL data for a blazar model with the same parameters, except that $\Gamma = 5$, $\ell'_e = 10^{42}$ ergs s^{-1} sr $^{-1}$, and synchrotron/SSC statistics.

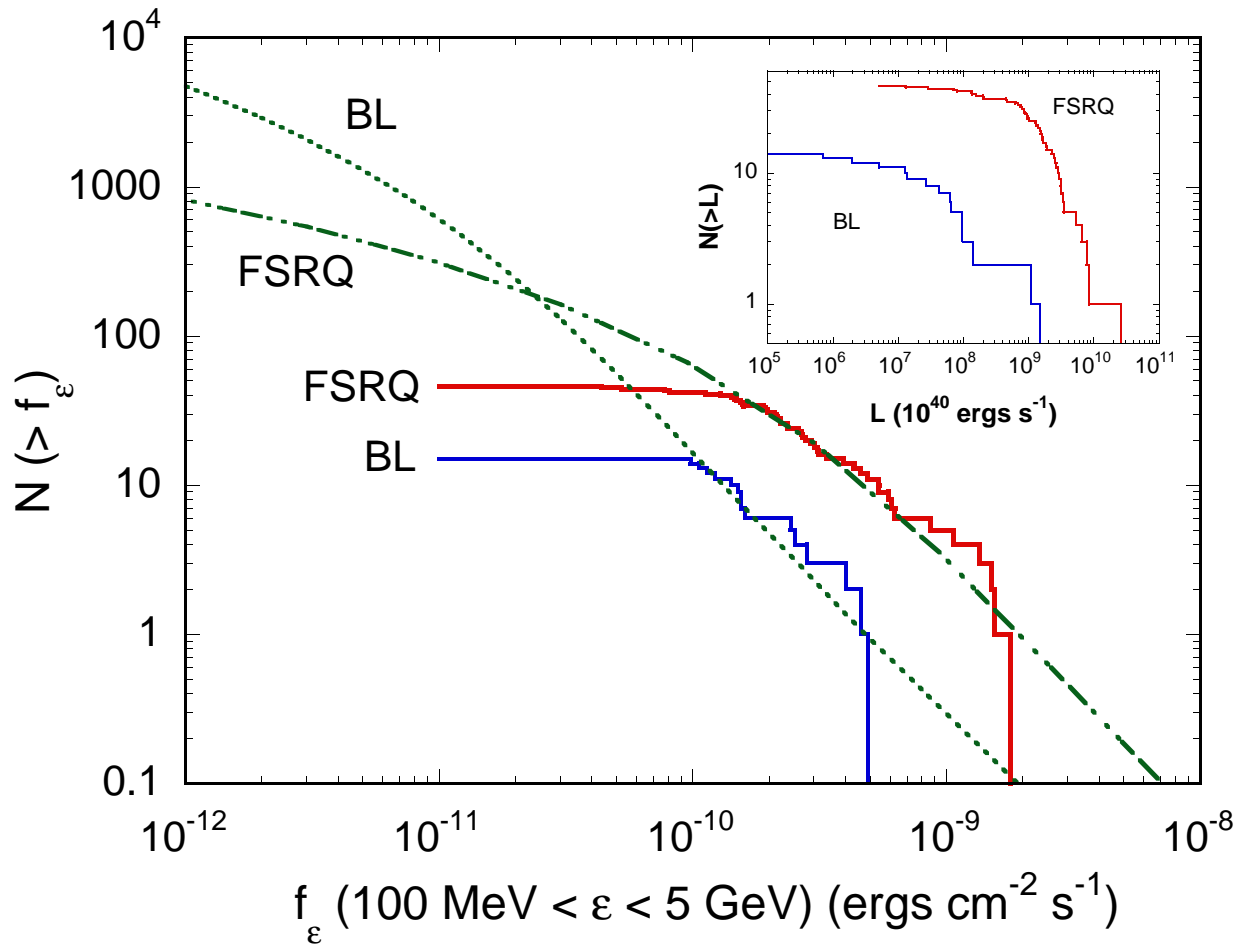


Fig. 2.— EGRET observations of $\gtrsim 100$ MeV νF_ν peak flux size distribution of blazars, versus model size distributions for FSRQ and BL blazars with parameters given in the caption to Fig. 1. The inset shows the size distribution for peak apparent blazar luminosities.

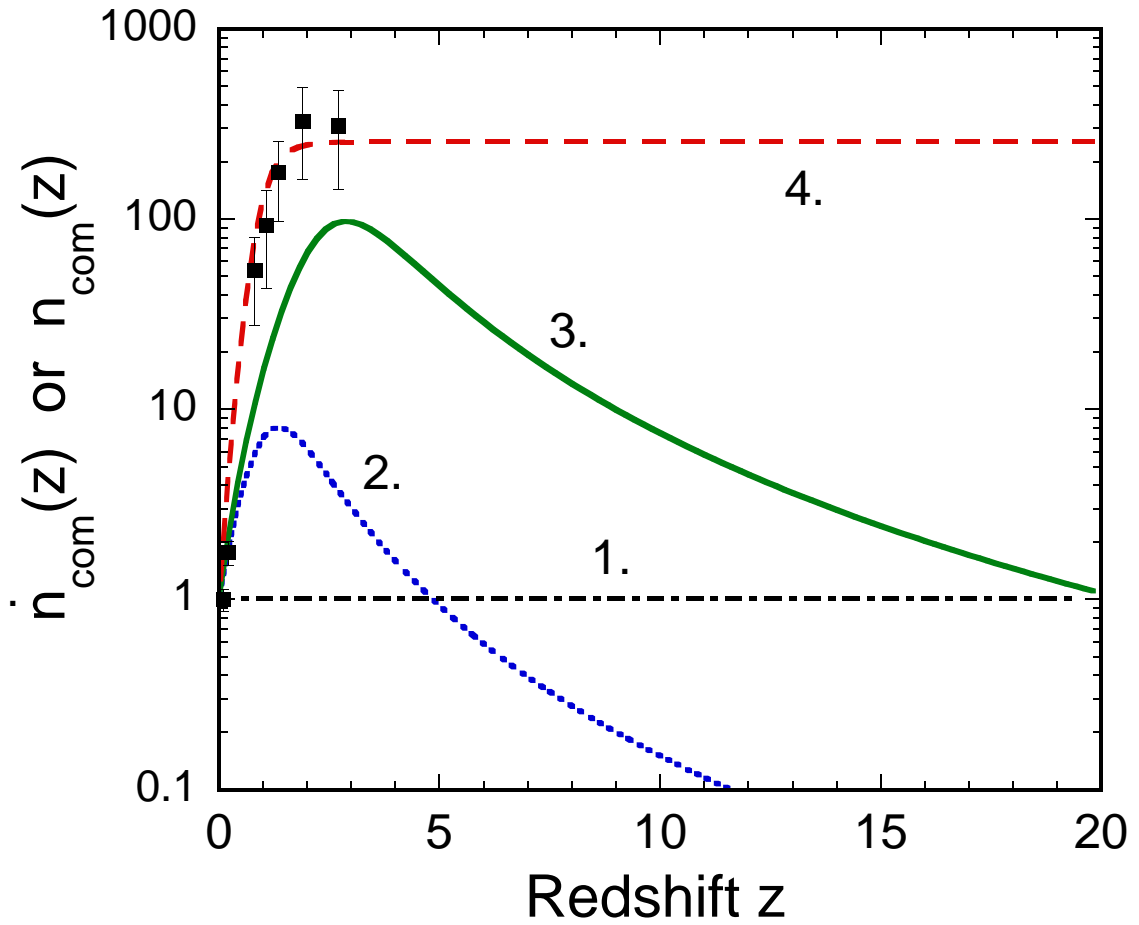


Fig. 3.— Model blazar formation rates (BFRs) used in this study. Curve 1 is the constant comoving rate, curves 2 and 3 are star formation rate histories without and with extinction corrections, respectively, and curve 4 is a rate proportional to the IR energy density inferred from IR galaxies (data points from Sanders 2004). The density evolution of the comoving blazar source rate-density $\dot{n}_{com}(z)$ or comoving blazar source density $n_{com}(z)$ is assumed to be proportional to one of these functions.

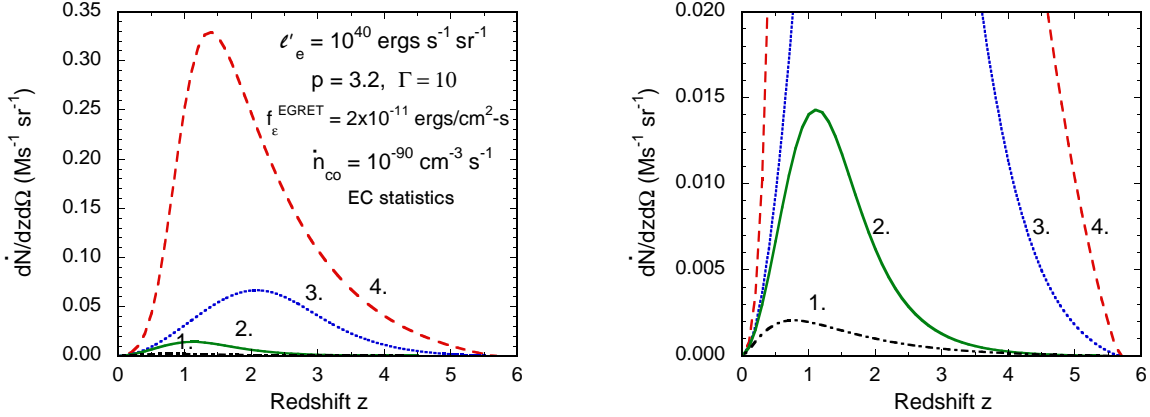


Fig. 4.— Dependence of the blazar redshift distribution on the different BFRs shown in Fig. 2. The EGRET γ -ray telescope is simulated with a flux threshold $f_\epsilon = 2 \times 10^{-11} \text{ ergs cm}^{-2} \text{ s}^{-1}$ at $\epsilon \approx 200$, corresponding to a two-week integrated EGRET νF_ν flux threshold of $\approx 10^{-10} \text{ ergs cm}^{-2} \text{ s}^{-1}$ between 100 MeV and 5 GeV. The linear scale on the left shows better BFR3 and 4 (left), and on the right shows better BFR 1 and 2, for a standard model blazar with parameters indicated.

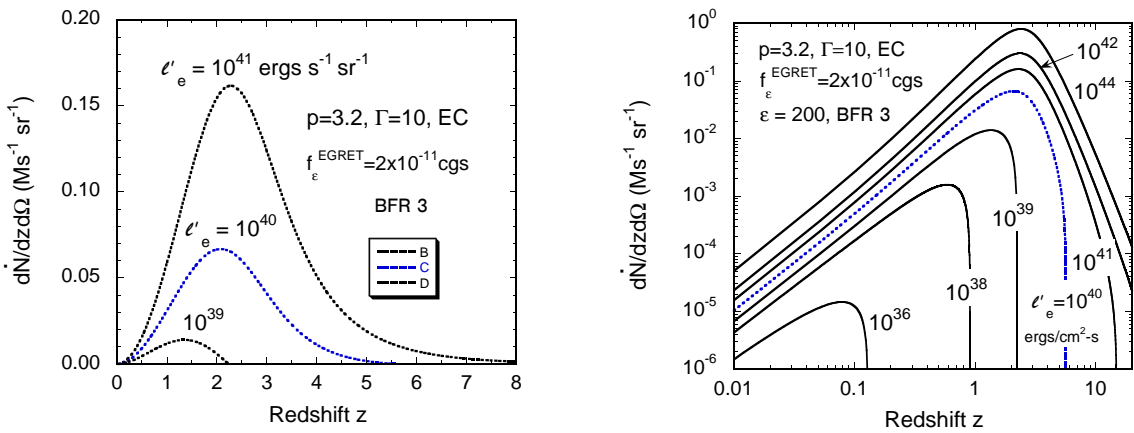


Fig. 5.— Model redshift distributions for standard model blazars with BFR 3 for different values of the comoving power. (left) Linear scale, with ℓ'_e changed by only 2 orders of magnitude. (right) Log-log scale, with ℓ'_e varying by 8 orders of magnitude.

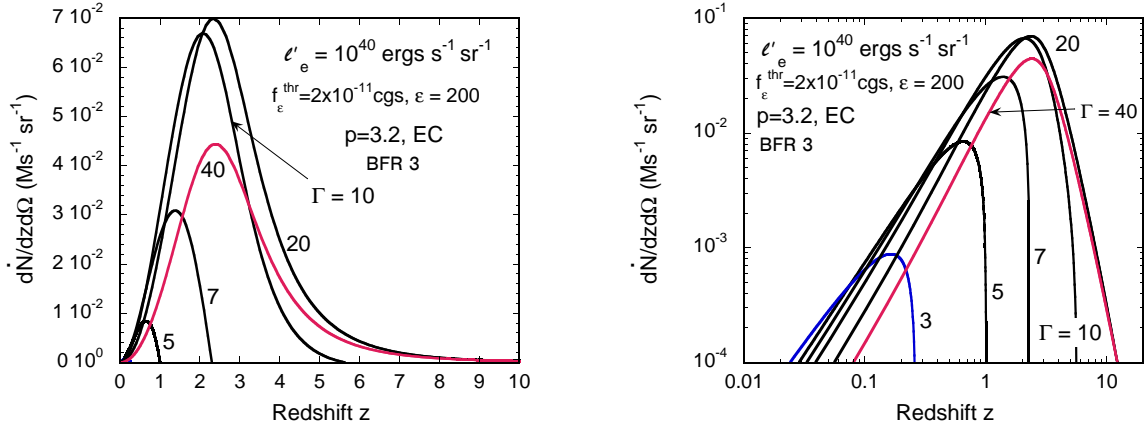


Fig. 6.— Blazar redshift distribution for a standard model blazar with BFR 3 and Γ varied from 3 to 40. (left) Linear scale. (right) Logarithmic scale.

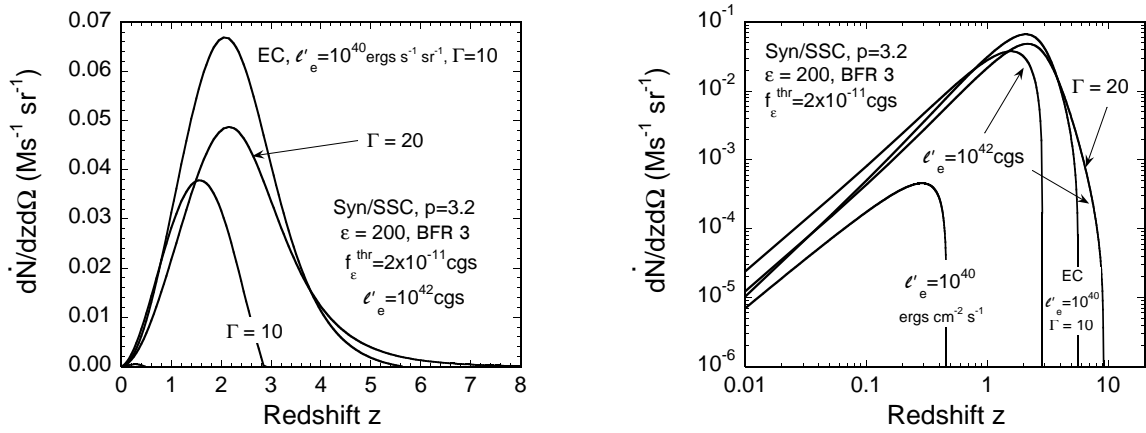


Fig. 7.— Blazar redshift distribution for a model blazar with $\Gamma = 10$, EC statistics, and EGRET detection properties (upper blue dotted curve) compared with results for synchrotron statistics, with different directional jet powers ℓ'_e and Γ factors as labeled. (left) Linear scale. (Right) Logarithmic scale.

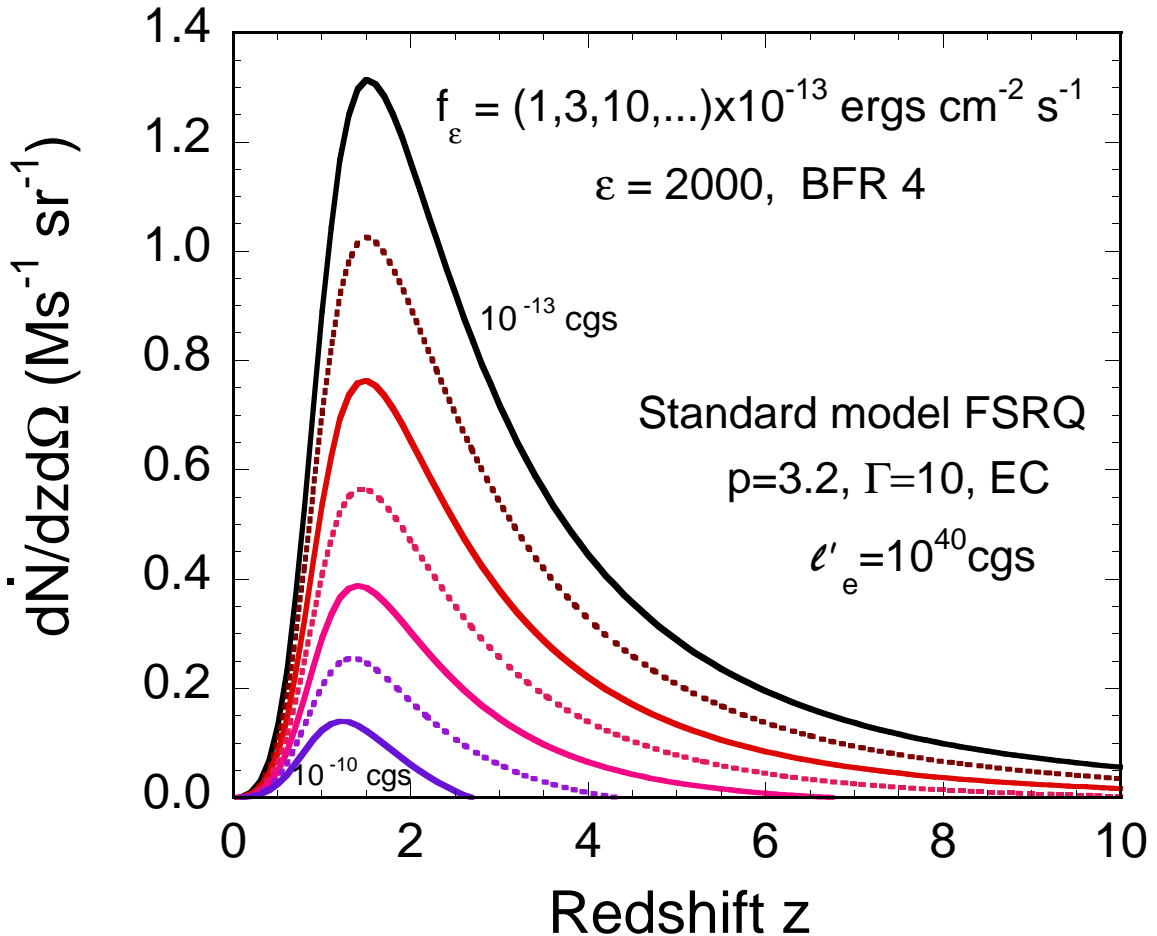


Fig. 8.— Redshift distribution for a standard model FSRQ blazar with $\Gamma = 10$, EC statistics, and BFR 4 as observed with an idealized γ -ray telescope with observing frequency $\epsilon = 2000$ at different flux sensitivity thresholds f_ϵ .

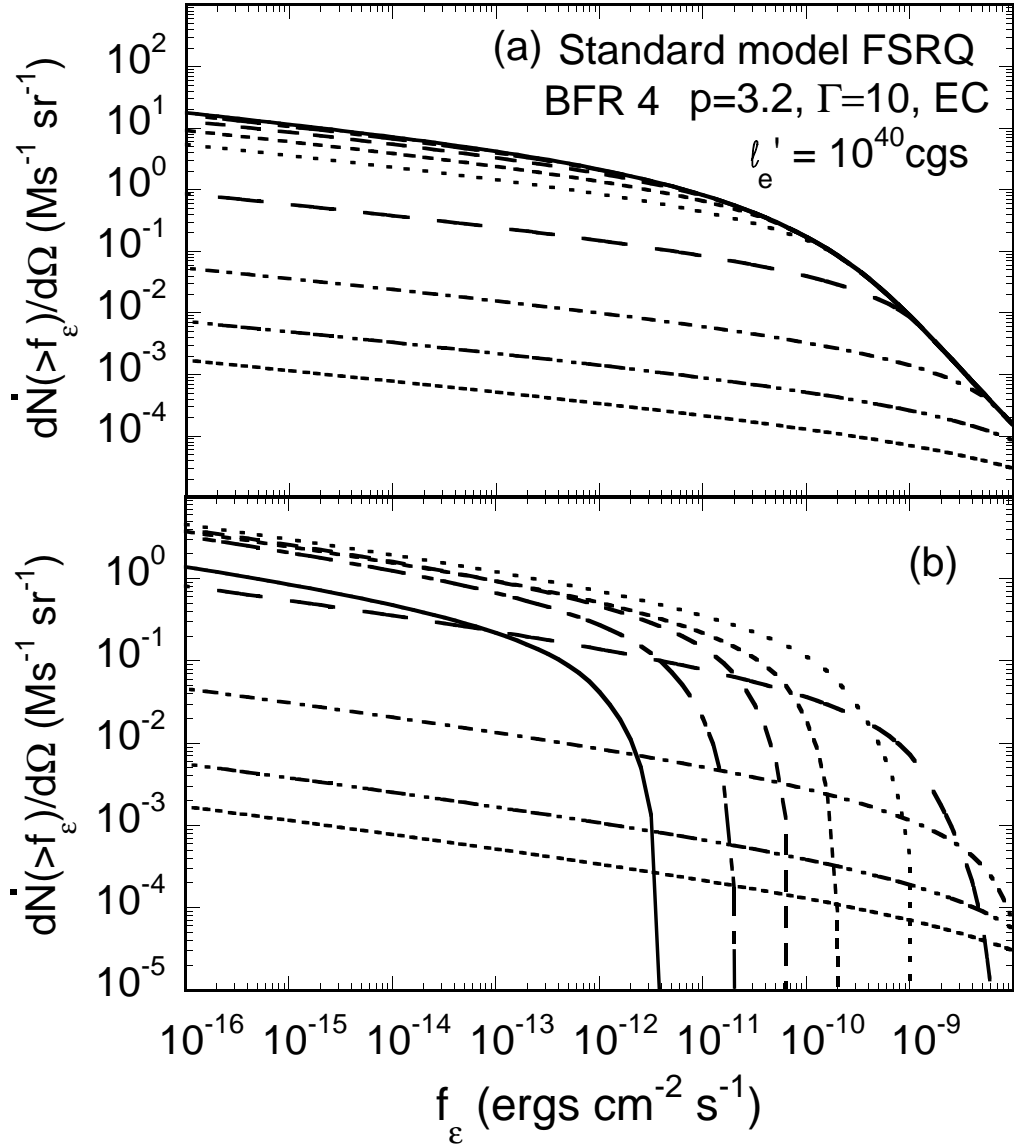


Fig. 9.— Size distributions for a standard model FSRQ blazar with $\Gamma = 10$, EC statistics, and BFR 4. Solid curve in upper panel (a) is size distribution for all detected blazars. Successively lower curves in panel (a) are size distributions for blazars with maximum redshifts $z_{max} = 5, 3, 2, 1, 0.5, 0.3, 0.2$, and 0.1 . (b) Size distributions of a standard model FSRQ for redshift ranges $10 < z < 20$ (solid), $5 < z < 10$ (long dot-dashed), $3 < z < 5$ (dashed), $2 < z < 3$ (short-dashed), $1 < z < 2$ (dotted), $0.5 < z < 1$ (long-dashed), $0.3 < z < 0.5$ (short dot-dashed), $0.2 < z < 0.3$ (double dot-dashed), and $z < 0.2$ (bottom curve).

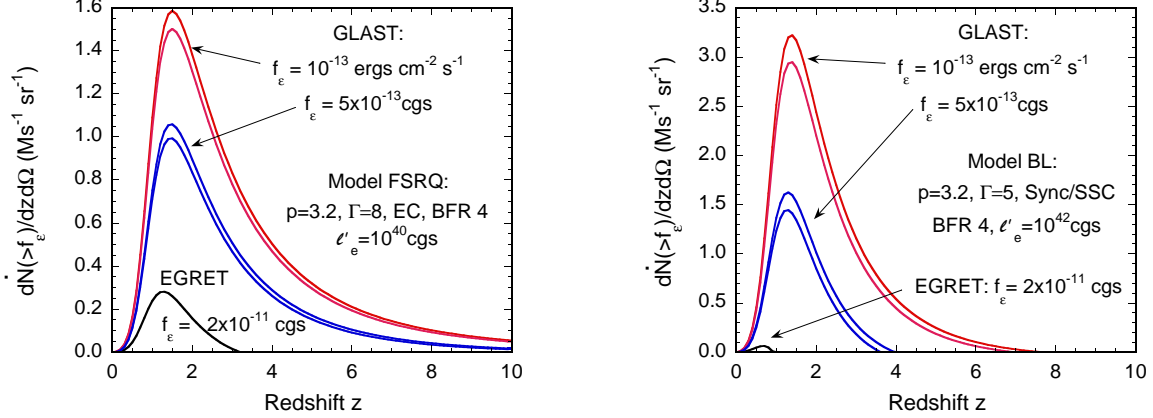


Fig. 10.— Model FSRQ (left panel) and BL (right panel) redshift distribution for model FSRQ and BL blazars with parameters given in the figure legend. GLAST predictions for $f_\epsilon = 5 \times 10^{-13} \text{ ergs cm}^{-2} \text{ s}^{-1}$ and for $f_\epsilon = 1 \times 10^{-13} \text{ ergs cm}^{-2} \text{ s}^{-1}$ are shown by the middle and upper pairs of curves, respectively. The observing frequency is $\epsilon = 200$ and $\epsilon = 2000$ for the higher and lower curve, respectively, in each pair of curves.

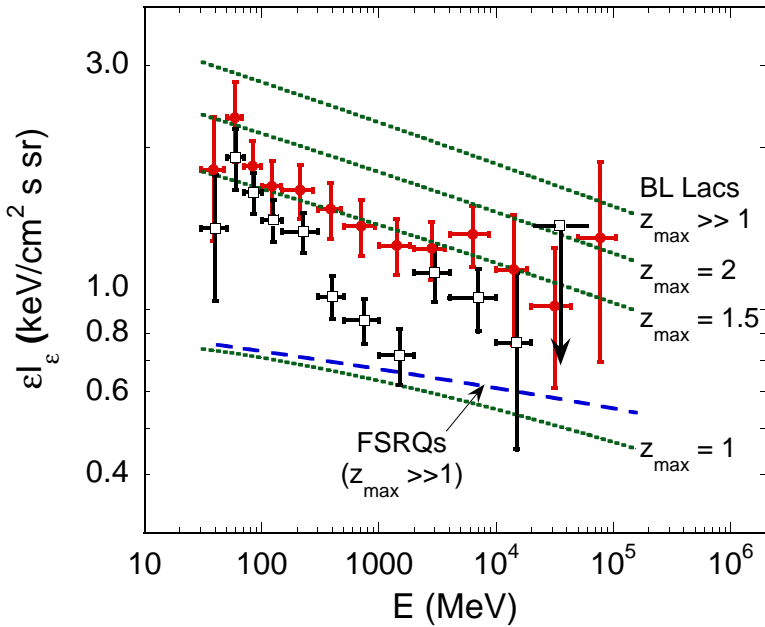


Fig. 11.— The diffuse γ -ray background intensity measured with the EGRET is shown by the filled data points (Sreekumar et al. 1998), and the DEGRB after subtraction of all galactic radiation fields is shown by the open data points (Strong et al. 2004). The dashed curve gives the diffuse intensity from unresolved FSRQs, and the dotted curves give the diffuse intensity from unresolved BLs, which are integrated to a maximum redshift as labeled. Blazars are assumed to be unresolved for fluxes weaker than $f_\epsilon \leq 2 \times 10^{-11} \text{ ergs cm}^{-2} \text{ s}^{-1}$ at $\epsilon = 200$.

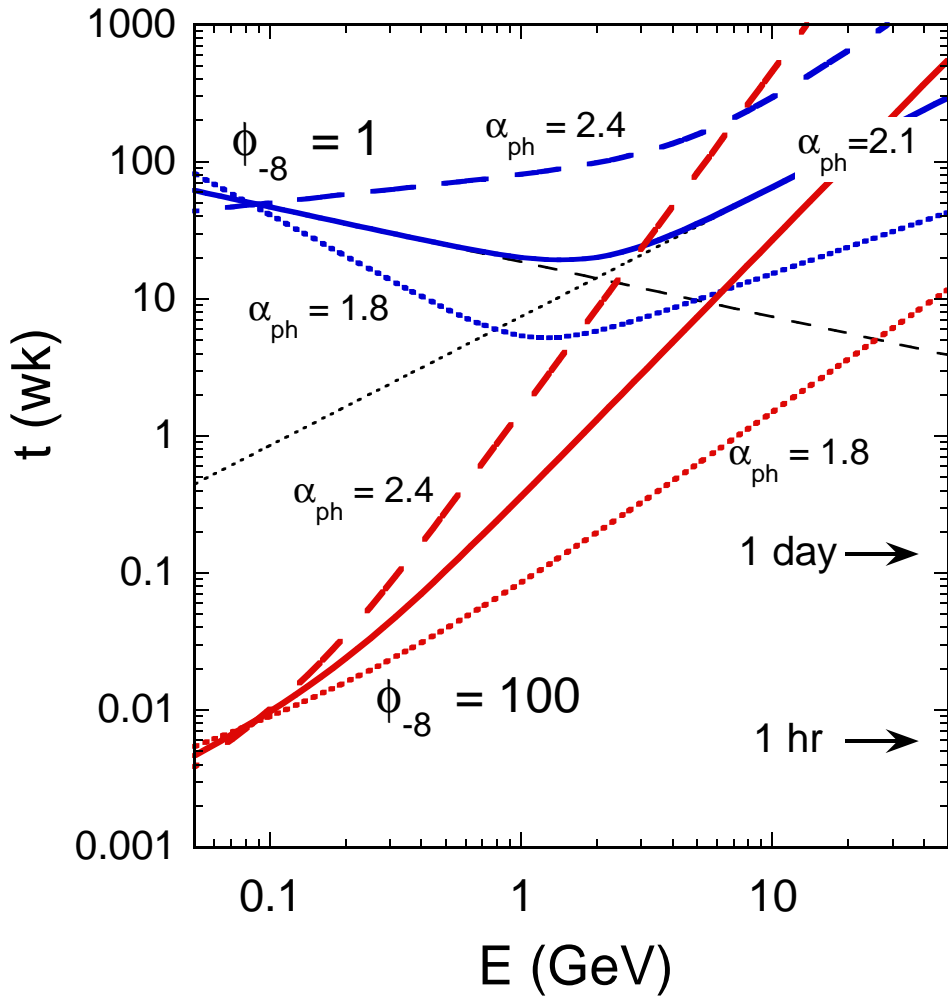


Fig. 12.— Time required for GLAST in the scanning mode to detect a source at integral flux levels $\phi_{-8} = 1$ and $\phi_{-8} = 100$ when integrating signal above energy E , for sources with photon spectral indices $\alpha_{ph} = 2.4$ (thick long-dashed curves), $\alpha_{ph} = 2.1$ (thick solid curves), and $\alpha_{ph} = 1.8$ (thick dotted curves). Light dashed and dotted lines show the time required to detect a source from signal and background limits, respectively, for $\phi_{-8} = 1$ and $\alpha_{ph} = 2.1$.